# Data-driven gap filling and spatio-temporal filtering of the GRACE/GRACE-FO records

Louis-Marie Gauer[1], Kristel Chanard[1], and Luce Fleitout[2]

[1]IPGP
[2]ENS-CNRS

November 23, 2022

**Abstract**

Gravity Recovery And Climate Experiment (GRACE) and GRACE-Follow On (GRACE-FO) global monthly measurements of Earth's gravity field have led to significant advances in the quantification of mass transfer on Earth. Yet, a long temporal gap between missions prevents interpretation of long-term mass variations. Moreover, instrumental and processing errors translate into large non-physical stripes polluting geophysical signals. We use Multichannel Singular Spectrum Analysis (M-SSA) to overcome both issues by exploiting spatio-temporal information of multiple Level-2 GRACE/GRACE-FO solutions. We statistically replace missing data and outliers using iterative M-SSA on Equivalent Water Height (EWH) time series processed by CSR, GFZ, GRAZ, and JPL to form a combined evenly spaced solution. Then, M-SSA is applied to retrieve common signals between each EWH time series and its neighbours to reduce residual spatially uncorrelated noise. We develop a complementary filter, based on the residual noise between fully processed data and a parametric fit to observations, to further reduce persisting stripes. Comparing GRACE/GRACE-FO M-SSA solution with SLR low-degree Earth's gravity field and hydrological model demonstrates its ability to statistically fill missing observations. Our solution reaches a noise level comparable to mass concentration (mascon) solutions over oceans, without requiring \textit{a priori} information or regularisation. While short-wavelength signals are hampered by filtering of spherical harmonics solutions or challenging to capture using mascon solutions, we show that our technique efficiently recovers localized mass variations using well-documented mass transfers associated with reservoir impoundments.

# Data-driven gap filling and spatio-temporal filtering of the GRACE/GRACE-FO records

**Louis-Marie Gauer[1], Kristel Chanard[1], Luce Fleitout[2]**

[1]Université de Paris, Institut de physique du globe de Paris, CNRS, IGN, Paris, France
[2]Laboratoire de Géologie, École Normale Supérieure, Université PSL, CNRS, Paris, France

## Key Points:

- Gap filling and spatio-temporal filtering of the GRACE/GRACE-FO gravity fields are performed using M-SSA
- The Lobe-Edge spectral filter, which complements the widely used DDK decorrelation, helps reducing striping noise
- The final solution shows minimal noise content and potential for retrieving smaller scale signals compared to others

## Plain language summary

The Gravity Recovery and Climate Experiment (GRACE) and GRACE Follow-On (GRACE-FO) satellite global measurements of changes in the Earth gravity field uniquely observe mass variations within and between the atmosphere, oceans, continental hydrology and ice. Yet, monthly data are polluted by noise in a North/South striping pattern, likely related to systematic errors and imperfect correction models. Moreover, the gap between missions prevents from measuring rates of mass changes which are essential for quantifying and understanding the impacts of climate change and human activity on the evolving ice and freshwater resources. To overcome both issues, we present a new post-processing procedure of the GRACE/GRACE-FO gravity fields, that has potential for an improved spatial resolution. This is accomplished using a mathematical method to exploit spatio-temporal correlations in the gravity time series. We perform gap filling based on the most statistically correlated signals and efficiently filter gravity fields by discarding the less correlated ones. The final GRACE/GRACE-FO solution shows low residual noise level over the oceans and is able to retrieve short-wavelengths signals such as reservoir impoundments or small glaciers, which are often smeared out over large regions or masked out by other processing methods.

Corresponding author: Louis-Marie Gauer, `gauer@ipgp.fr`

## Abstract

Gravity Recovery And Climate Experiment (GRACE) and GRACE-Follow On (GRACE-FO) global monthly measurements of Earth's gravity field have led to significant advances in the quantification of mass transfer on Earth. Yet, a long temporal gap between missions prevents interpretation of long-term mass variations. Moreover, instrumental and processing errors translate into large non-physical stripes polluting geophysical signals. We use Multichannel Singular Spectrum Analysis (M-SSA) to overcome both issues by exploiting spatio-temporal information of multiple Level-2 GRACE/GRACE-FO solutions. We statistically replace missing data and outliers using iterative M-SSA on Equivalent Water Height (EWH) time series processed by CSR, GFZ, GRAZ, and JPL to form a combined evenly spaced solution. Then, M-SSA is applied to retrieve common signals between each EWH time series and its neighbours to reduce residual spatially uncorrelated noise. We develop a complementary filter, based on the residual noise between fully processed data and a parametric fit to observations, to further reduce persisting stripes. Comparing GRACE/GRACE-FO M-SSA solution with SLR low-degree Earth's gravity field and hydrological model demonstrates its ability to statistically fill missing observations. Our solution reaches a noise level comparable to mass concentration (mascon) solutions over oceans, without requiring *a priori* information or regularisation. While short-wavelength signals are hampered by filtering of spherical harmonics solutions or challenging to capture using mascon solutions, we show that our technique efficiently recovers localized mass variations using well-documented mass transfers associated with reservoir impoundments.


## 1 Introduction

From March 2002 to October 2017, the Gravity Recovery And Climate Experiment (GRACE) has measured changes in the Earth's gravity field (Tapley et al., 2004). The GRACE mission included two satellites in a low, near-circular, near-polar orbit following each other at a distance of approximately 220 km. When the leading satellite passed over a sizeable mass, it was pulled slightly more towards the mass than the trailing satellite and orbits were perturbed differently. By precisely measuring variations in the intra-satellites distance, it was possible to weigh the Earth's mass variations through the differential gravitational pull on the two satellites. GRACE proved relevant and rapidly became an essential tool for monitoring the movements of mass within and between Earth's atmosphere, oceans, land and ice sheets. In fact, over the past decades, GRACE has provided insights in various fields, from geophysics to hydrology. For example, observations of mass variations derived from GRACE have been used to monitor global and regional terrestrial water storage (Syed et al., 2008; Longuevergne et al., 2013; Long et al., 2015; J. Chen et al., 2016), global ocean mass changes (Morison et al., 2007; Wouters et al., 2011; Gardner et al., 2013), ocean bottom pressure (Johnson & Chambers, 2013), or recent ice melting (Luthcke et al., 2013; Wouters et al., 2019; Velicogna et al., 2020). Moreover, GRACE revealed valuable information on processes occurring within the solid Earth, including the seismic cycle (Panet et al., 2007; J. L. Chen et al., 2007; Bouih et al., 2022) or Glacial Isostatic Adjustement (GIA; Steffen et al. (2008); Velicogna & Wahr (2013)). The success of the GRACE mission overall motivated a follow-up mission, GRACE-Follow On (GRACE-FO; (Flechtner et al., 2016; Landerer et al., 2020)), launched in May 2018. Unfortunately a significant temporal gap between the two missions exists, in addition to the increasing missing observations towards the end of the GRACE mission. Yet, having a time series of measurements of sufficient length, consistency and continuity is vital to investigate long-term gravity changes occurring with the solid Earth processes and, even more so, monitor climate-related mass variations, such as the ongoing evolution of ice sheets and glaciers or land water storage.

Unfortunately, due to the orbital geometry of both missions, observations bear a high-sensitivity in the North-South direction. As a result, instrumental errors, shortcomings in the oceanic and atmospheric gravity field correction models (Seo et al., 2006, 2007), or any other processing error translate into a distinctive noise with a North-South striping pattern, limiting GRACE measurements quality and potential use for even more geophysical applications (Han et al., 2004; Thompson et al., 2004; Swenson & Wahr, 2006). In order to reduce this characteristic noise, several signal processing methods have been developed using various mathematical tools (Werth et al., 2009). First, North-South stripes polluting the gravity fields derived from raw GRACE observations, expressed in terms of Stokes coefficients of their Spherical Harmonics (SH) decomposition, can be removed using different filtering methods. Examples of post-processing methods include: Gaussian filters (Wahr et al., 2004; Seo et al., 2007), a combination of them (Guo et al., 2010), or the widely used DDK decorrelation filters (Kusche, 2007; Kusche et al., 2009). DDK filters aim at reducing correlations between Stokes coefficients of the gravity field SH decomposition via matricial and gaussian filters. Since all filtering methods require a compromise between smoothing — hence spatial resolution and signal attenuation — and reducing noise, DDK filters offer a family of filters (DDK1 to DDK8), corresponding to different levels of filtering. To further reduce noise in the GRACE and GRACE-FO derived gravity fields, partly due to limitations in processing strategies, solutions provided by various processing centres can be combined at the observations level (COST-G; Jäggi et al. (2020)), or averaged during post-processing (Sakumura et al., 2014). Alternatively, the GRACE mass concentration (mascons) solutions have been developed to propose leakage-suppressed and ready to use solutions (Luthcke et al., 2013; Watkins et al., 2015; Save et al., 2016). However, achieving these solutions requires the introduction of potentially biased *a priori* information on the spatio-temporal distribution of the signal or noise structure, or regularisation in the least-squares gravity inversion (Loomis et al., 2019).

In parallel, statistical signal-processing techniques, namely statistical decomposition methods, have been used to identify patterns of variability in the GRACE time series. Most of these methods aim at retaining only a set of patterns representing most of the geophysical signal variability, in order to filter out less correlated parts of the signal dominated by North-South stripes. In particular, eigenspace techniques have been commonly applied to isolate geophysical signals in GRACE derived gravity field time series. First, Principal Component Analysis (PCA; Lorenz (1956)), also called Empirical Orthogonal Function (EOF) analysis, has been used to extract dominant orthogonal modes from GRACE data, either for filtering noise (Chambers, 2006; Schrama et al., 2007; Chambers & Willis, 2008; Wouters & Schrama, 2007), or extracting signals of interest (De Viron et al., 2006; Rangelova et al., 2007; Rangelova & Sideris, 2008; Rieser et al., 2010). However, the physical interpretation of modes extracted using PCA can be biased by the superposition of independent source signals in the time series. Therefore, Independent Component Analysis (ICA), which aims at separating dominant modes based on the assumed statistical independence of signal sources, has been preferred over PCA (Frappart et al., 2010; Forootan & Kusche, 2012). Yet, both PCA and ICA only use information between existing time series, ignoring the potential lagged correlations between time series, and are thus limited to stationary processes. If they are efficient at separating signals with various temporal behaviours, capturing the spatio-temporal evolving nature of geophysical signals encompassed in the GRACE data remains challenging (Forootan et al., 2014). Incorporating any lagged information on a single time series is fortunately possible using Singular Spectrum Analysis (SSA; Vianna et al. (2007); X. Wang et al. (2011)). Moreover, the Multichannel (or multivariable)-SSA (M-SSA, (Ghil et al., 2002)), a generalization of both the PCA and SSA, which uses time-lagged observations and multiple time series, is particularly well adapted to capture the complex spatio-temporal modes of variability of the GRACE data (Zotov & Shum, 2010; Rangelova et al., 2012; F. Wang et al., 2020). In fact, both Prevost et al. (2019) and F. Wang et al. (2020) have shown the potential of M-SSA as a data-adaptive filtering tool for GRACE Level-2 solutions reducing processing-specific errors and noise content.

The large number of missing observations towards the end of the GRACE mission and the 11-month observational gap between missions limit the potential use of GRACE and GRACE-FO data to their full potential. Consequently, efforts have been carried out to fill temporal observational gaps of the GRACE gravity fields. First, independent observations have been used to fill GRACE data gaps. Particularly, direct observations from Satellite Laser Ranging (SLR) or Global Positioning System (GPS) receivers onboard Swarm satellites can be exploited to reconstruct low-degree of the Earth's gravity field (Jäggi et al., 2016; Lück et al., 2018; Richter et al., 2021). Inversions of deformation fields, as measured for example by Global Navigation Satellite System (GNSS) global networks can also lead to low-degree gravity field estimates through loading theory (Rietbroek et al., 2014; Chanard et al., 2018; Wu et al., 2020). Yet, independent data may contain specific technique-related errors or other physical processes that can bias GRACE gravity field gap filling (Dong et al., 2002; Mémin et al., 2020). GRACE temporal gaps can be reconstructed using data-adaptive statistical techniques, such as SSA and M-SSA, to decompose the time series into a subset of temporal or spatio-temporal components then used to reconstruct missing observations (Kondrashov & Ghil, 2006a). SSA has been used in an iterative approach to perform gap filling on time series of the coefficients of GRACE gravity field SH decomposition (Prevost et al., 2019; Li et al., 2019; Yi & Sneeuw, 2021). M-SSA has also proven its ability to reconstruct missing observations, at least for low-degree SH coefficients of the Earth's gravity field, using Swarm observations (F. Wang et al., 2021), or part of the gravity variations, namely climate-driven water storage changes, using precipitation and temperature models (Yang et al., 2021; Humphrey & Gudmundsson, 2019). Recently, machine learning techniques have also been employed to perform gap filling in and between GRACE and GRACE-FO observational periods. Examples include reconstructing the terrestrial water component of the gravity field using an hydroclimatic data-driven Bayesian convolutional neuronal network (Mo et al., 2022) or an algorithm combining M-SSA with an artificial neural network (Lai et al., 2022). Unfortunately, these methods are more complex, computationally more challenging than classical statistical methods, and often limited to terrestrial water storage applications discarding mass change related to solid Earth processes.

In this study, we propose an innovative post-processing strategy for gap filling, combining and filtering four Level-2 GRACE/GRACE-FO gravity field solutions using a unique statistical method, the M-SSA. We first present, in Section 2, the GRACE/GRACE-FO data used. In Section 3, after describing the M-SSA method, we explicit our post-processing strategy and present results. The method includes an iterative M-SSA algorithm for observational gap filling using multiple Level-2 GRACE and GRACE-FO solutions, with synthetic tests for validation, a new filter in the spectral domain and a M-SSA-based spatio-temporal filtering procedure to efficiently reduce the persistent North-South stripes. Then, in Section 4, we first validate the M-SSA gap filling algorithm by comparing results to independent observations, namely SLR for low-degree SH coefficients and hydrological model. Finally, we compare our results with published GRACE and GRACE-FO solutions, using different processing strategies. In particular, we confront noise content of the gravity field solutions over the oceans, and assess solutions performances for a selection of regional examples, including hydrological mass balance for reservoir impoundments.

# 2 GRACE and GRACE-FO Level-2 solutions

## 2.1 GRACE and GRACE-FO datasets

The GRACE and more recently, the GRACE-FO missions provide monthly maps of the Earth's gravity field with a spatial resolution of a few hundreds kilometres (Tapley et al., 2004; Landerer et al., 2020). Unfortunately a substantial 11-month temporal gap, from June 2017 to May 2018, exists between missions (Figure 1). The raw Level-1 data are processed by several processing centres to provide monthly Level-2 solutions

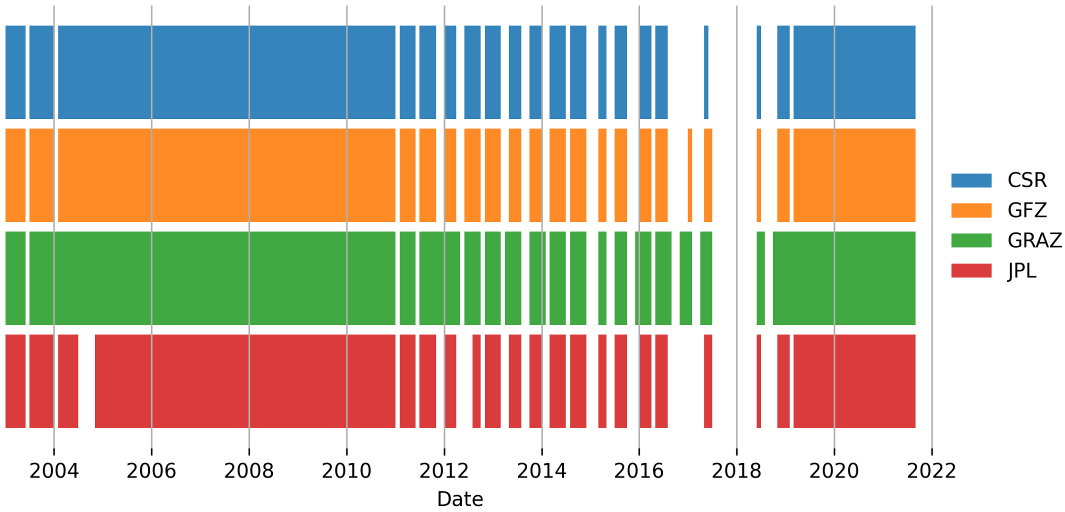


Figure 1: Temporal sampling of the Level-2 monthly GRACE and GRACE-FO solutions provided by the CSR, GFZ, GRAZ and JPL processing centres.

of the Earth's gravitational field. These solutions are distributed in terms of Stokes coefficients of the Earth's gravity field Spherical Harmonics (SH) decomposition. Differences in processing strategies yield two major consequences. First, raw Level-1 monthly signal to noise ratio requirements cause differences in Level-2 temporal sampling between processing centres (Figure 1). Then, noise discrepancies arise from differences in processing strategies (Swenson & Wahr, 2002; Sakumura et al., 2014). In this study, we take advantage of Level-2 gravity field solutions from 4 different processing centres, expressed in Stokes coefficients of the SH decomposition, for which specifications are presented in Table 1. Note that while the maximum degree of the gravity field SH decomposition provided by the centres is 96, we use a 89 cut-off degree to ensure a corresponding 1-by-1 degree longitude and latitude grid. Since degrees 90 to 96 are low amplitude and largely affected by noise, our solution is not impacted by the truncation. We focus our study on the 2003-01 to 2017-06 GRACE period, discarding the noisier starting and ending periods of the mission, and on the 2018-06 to 2021-08 GRACE-FO period. The non-observable degree-1 SH geocenter gravity coefficients are accounted for using an average of coefficients provided for each the GFZ, JPL and CSR solutions in Technical Note 13 (TN-13; Swenson et al. (2008); Sun et al. (2016)). Moreover, $C_{2,0}$ Earth oblateness and $C_{3,0}$ gravity coefficients, which are difficult to observe due to the near polar orbit of the GRACE and GRACE-FO missions, are substituted with satellite laser ranging (SLR) observations according to Technical Note 14 (TN-14; J. Chen et al. (2005); Loomis et al. (2020)). Finally, all GRACE and GRACE-FO solutions used in this study have been corrected for non-tidal high-frequency atmospheric and oceanic mass variation models, namely the Atmosphere and Ocean Dealiasing Level-1B (AOD1B) model (Dobslaw et al., 2017).

### 2.2 GRACE and GRACE-FO data post-processing

To investigate variations in the Earth's gravity field, we first remove its mean value, estimated over the 2003-2021 period, from each Level-2 solution. Consequently, the characteristic nonphysical North-South elongated striping patterns, arising from instrumental errors or shortcomings in the gravity field correction models of known phenomena, dominate both GRACE and GRACE-FO solutions. Figures 2a and 2b show examples of the resulting GRACE and GRACE-FO gravity fields, expressed in Equivalent Water Height (EWH) for July 2008 and 2019 respetively. The large amplitude of the North-

| **Centre** | **Version** | **Max. degree** | **Cut-off degree** |
|---|---|---|---|
| CSR | RL06 | 96 | 89 |
| GFZ | RL06 | 96 | 89 |
| GRAZ | ITSG 2018/ITSG operational | 96 | 89 |
| JPL | RL06 | 96 | 89 |

Table 1: GRACE and GRACE-FO Level-2 solutions from the CSR, GFZ, GRAZ and JPL processing centres used in this study, maximum degree of the solutions spherical harmonic decomposition and truncation degree used in this study.

South striping artefacts emphasizes the necessity for filtering the GRACE and GRACE-FO gravity fields prior to any geophysical application (Sakumura et al., 2014). Here, we start by using the non-isotropic decorrelation filter, known as DDK (Swenson & Wahr, 2006; Kusche, 2007; Kusche et al., 2009). DDK is based on a regularisation using both the error and signal covariance information. The filter results in a single filtering matrix derived from the *a priori* error covariance of the August 2003 GRACE solution, that we apply to all GRACE and GRACE-FO monthly gravity fields. The filter offers 8 levels, from the strongest DDK1 to weakest DDK8 level, and impacts mainly the high degree coefficients of the SH decomposition which contain most of the stripping noise. An increase in the level of DDK filtering yield larger signal attenuation and leakage causing geophysical signals to smear out over larger regions. Thus, a compromise between solution filtering and noise reduction must be made. The usual compromise for geophysical applications is to use the mean of Level-2 solutions from the 3 official processing centres, CSR, GFZ and JPL, filtered by DDK5 (Sakumura et al., 2014) to efficiently remove North-South stripes while retaining geophysical signals at wavelengths $\lambda/2 \sim 180$ km (Figures 2c and 2d). Here, we rather apply the DDK7 filter, with $\lambda/2 \sim 145$ km (Figures 2e and 2f). Figure 3 shows an example of the impact of applying DDK5, compared to DDK7, on the intensity spectrum of the SH decomposition for the July 2008 GRACE CSR gravity field. DDK5 removes a larger part of the signal at high degrees which, while largely polluted by North-South striping artefacts, may still contain valuable geophysical information. Here, we first combine the DDK7 filter with a complementary filter, the Lobe-Edge (LE) filter presented in Section 3.4, that we develop based on the residual noise between fully processed data and a parametric fit to observations, to further reduce persisting stripes. All results presented in the following are based on a DDK7+LE filtering of the GRACE/GRACE-FO solutions, and results based on a DDK7 filtering only can be found in supplementary material. Next, we propose to perform additional filtering where no *a priori* information on the signal or noise structure is required to further reduce spurious noise while retaining smaller wavelengths signals and limit signal attenuation compared to the usual filtering compromise (Sakumura et al., 2014). By doing so, we intend to broaden possibilities of using GRACE and GRACE-FO in various geophysical domains.

## 3 Methodology

Once the GRACE and GRACE-FO data have been pre-processed with DDK7 filtering, solutions still contain significant North-South striping artefacts and missing data remain an issue for geophysical applications. The aim of the methodology developed in this study is to address both issues using a unique mathematical tool, namely the Multichannel-Singular Spectrum Analysis (M-SSA). The post-processing method is separated in two major steps: (1) data gap filling and (2) spatial filtering. In the following Section, we first briefly describe the M-SSA, and then detail both steps of the proposed methodol-

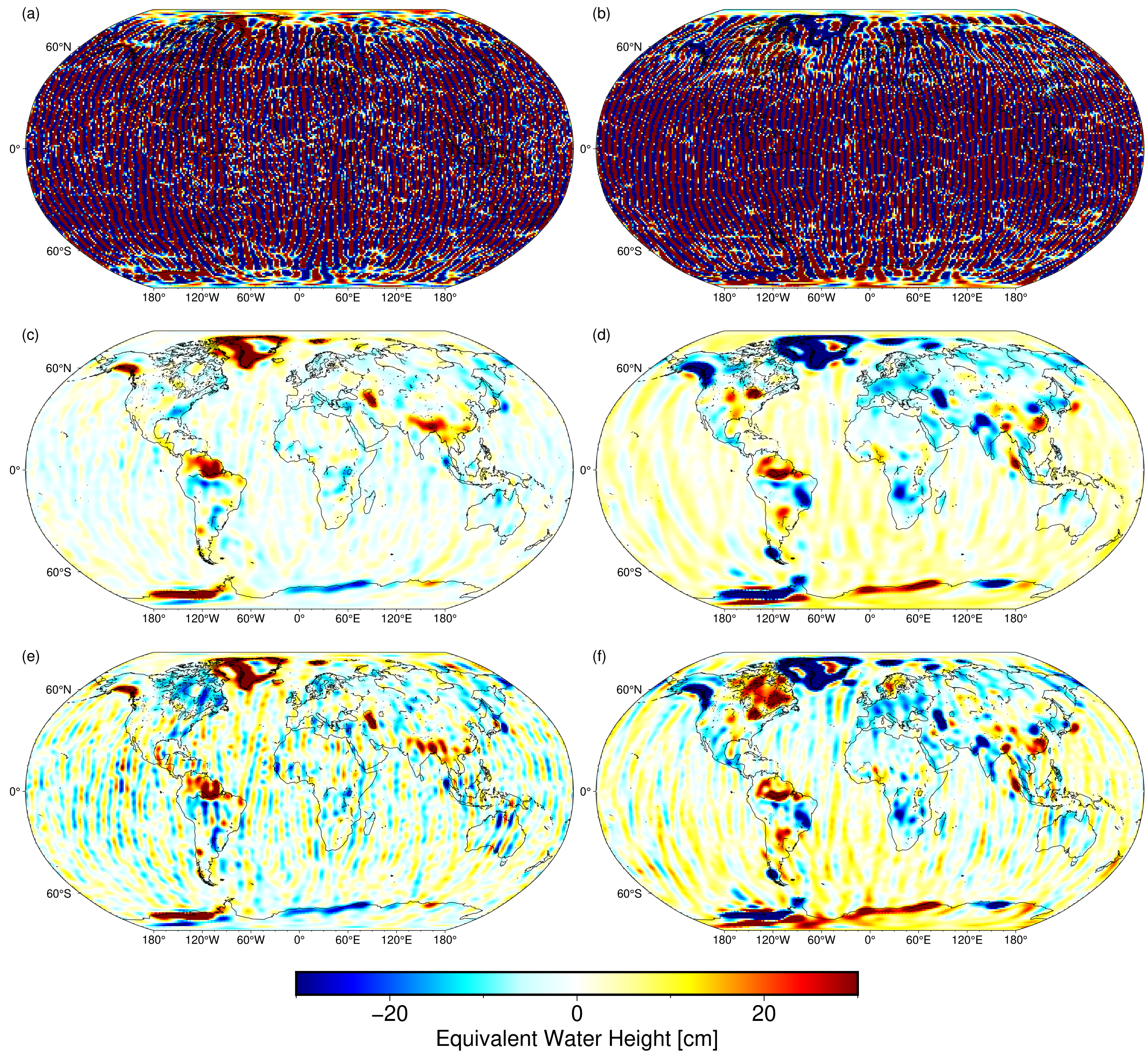


Figure 2: Mean of surface mass density anomaly of the unfiltered (a) and (b), the DDK5-filtered (c) and (d), and the DDK7-filtered (e) and (f) GRACE and GRACE-FO solutions processed by the CSR, GFZ, GRAZ and JPL centres, for July 2008 and July 2019 respectively, after removing its mean value estimated over the 2003-2021 period. Surface mass density anomalies are expressed in Equivalent Water Height (cm).

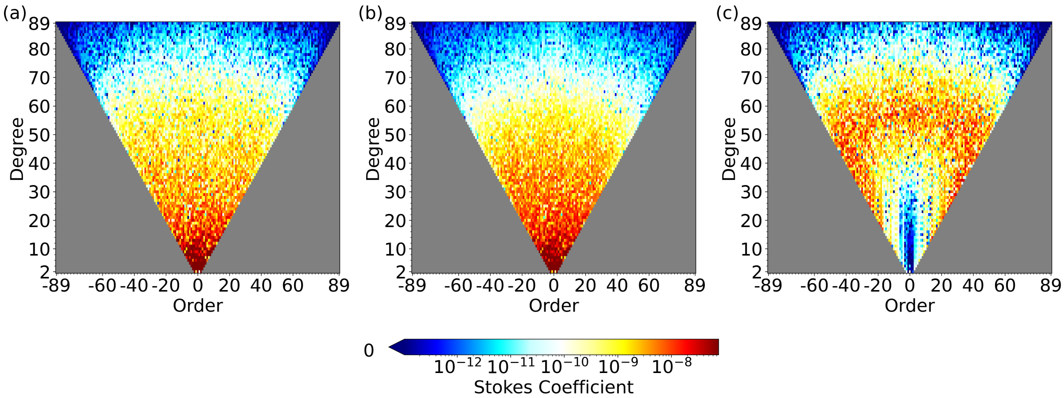


Figure 3: Stokes coefficients intensity spectra of the July 2008 GRACE CSR gravity filtered using (a) DDK5 and (b) DDK7 decorrelation filter. (c) shows the difference between DDK7 and DDK5 filtering applied to July 2008 GRACE gravity field.

ogy to fill and filter the pre-processed GRACE and GRACE-FO data as objectively as possible.

## 3.1 Multichannel Singular Spectrum Analysis (M-SSA)

The aim of M-SSA (Keppenne & Ghil, 1993; Plaut & Vautard, 1994) is to extract spatially and temporally correlated modes of the input signal channels, or time series, by using the covariance between them and between lagged delayed copies of them. Here, M-SSA is particularly interesting to (1) fill the GRACE and GRACE-FO data temporal gaps by using the correlations between multiple time series, and (2) reduce spurious uncorrelated noise in the data by retaining only the most correlated parts of the signal in space and time, without *a priori* information on the signal or noise structure. A brief description of the method is proposed in the following, and further information is provided by Ghil et al. (2002) in a more complete review of the methodology, including various examples of application.

### *Embedding procedure to estimate the multichannel trajectory matrix*

A multichannel time series with $L$ channels of length $N$, evenly spaced with sampling interval $\Delta T$ is defined as:

$$X_l = \{X_l(t), t \in [1, N]\}, l \in [1, L] \tag{1}$$

We first conduct the embedding, which maps one dimensional time series $X_l$ into a multi-dimensional series of copies of the original time series delayed over a sliding window of length $M$.

The embedding procedures leads to a trajectory matrix $\widetilde{X_l}$ defined for each time series $X_l$:

$$\widetilde{X_l} = \begin{pmatrix} X_l(1) & X_l(2) & \cdots & X_l(M) \\ X_l(2) & X_l(3) & \cdots & X_l(M+1) \\ \vdots & \vdots & \ddots & \vdots \\ X_l(N') & X_l(N'+1) & \cdots & X_l(N) \end{pmatrix} \tag{2}$$

Each row of the trajectory matrix relates to observations included in the sliding window of length $M$, and is delayed by $\Delta T$ from the preceding time row. This window is shifted until the last observation $N$ is reached. The trajectory matrix has a dimension of $N' \times$

$M$, where $N' = N - M + 1$ is the number of overlapping views of the series for each point in the channel (Ghil et al., 2002; Broomhead & King, 1986; Broomhead et al., 1986; Allen & Robertson, 1996). The multichannel trajectory matrix $\widetilde{X}$ can then be estimated as the concatenation of trajectory matrices for all $l$ time series included in the dataset as:

$$\widetilde{X} = \left(\widetilde{X}_1, \widetilde{X}_2, \cdots, \widetilde{X}_L\right) \tag{3}$$

***Estimating of the grand lag-covariance matrix***

Then, the grand lag-covariance matrix can be computed as:

$$\widetilde{C} = \frac{1}{N'}\widetilde{X}^t\widetilde{X} = \begin{pmatrix} C_{1,1} & C_{1,2} & \cdots & C_{1,L} \\ C_{2,1} & C_{2,2} & \cdots & C_{2,L} \\ \vdots & \vdots & \ddots & \vdots \\ C_{L,1} & C_{L,2} & \cdots & C_{L,L} \end{pmatrix} \tag{4}$$

where each block $C_{l,l'}$ is the covariance matrix between two time series $X_l$ and $X_l'$, given by:

$$C_{l,l'} = \frac{1}{N'}\widetilde{X_l}^t\widetilde{X_{l'}} \tag{5}$$

***Decomposing the grand lag-covariance matrix to determine eigenvalues and eigenvectors***

We solve the eigenvalues problem by diagonalising the $LM \times LM$ grand lag-covariance matrix $\widetilde{C}$ using singular value decomposition in order to compute eigenvalues $\lambda_k$ and eigenvectors $E^k$ as:

$$E^k\widetilde{C} = \lambda_k E^k \tag{6}$$

The $LM$ eigenvectors $E^k$ are called Spatio-Temporal Empirical Orthogonal Functions (ST-EOFs or EOFs for simplicity), and represent $L$ consecutive $M$-long segments $E_l^k$.

***Determining the Principal Components (PCs) of single-channel time series***

The $k^{th}$ spatio-temporal Principal Components (ST-PCs or PCs for simplicity), $\{A^k(t), t \in [1, N'], k \in [1, M \times L]\}$ are computed by projecting the $k^{th}$ row vector of $X_l$ time series onto the EOFs as:

$$A^k(t) = \sum_{j=1}^{M}\sum_{l=1}^{L} X_l(t + j - 1) \cdot E_l^k(j) \tag{7}$$

The $k^{th}$ PCs represent the common temporal modes of variability of the time series, with variance equal to the $k^{th}$ eigenvalues $\lambda_k$, sorted in decreasing order of the amount of the entire dataset variance captured by the corresponding PC.

***Computing the Reconstructed Components (RCs) and reconstructed time series***

Finally, the time series $X_l$ can be partially reconstructed using the PCs and EOFs (Plaut & Vautard, 1994). $R_l^k$, the partially reconstructed signal associated with the $k^{th}$ PC and

EOF is given by:

$$R_l^k(t) = \begin{cases} \dfrac{1}{t}\sum\limits_{j=1}^{t} A^k(t-j+1)\cdot E_l^k(j), & \text{if} \quad 1 \leqslant t \leqslant M-1 \\ \dfrac{1}{M}\sum\limits_{j=1}^{M} A^k(t-j+1)\cdot E_l^k(j), & \text{if} \quad M \leqslant t \leqslant N-M+1 \\ \dfrac{1}{N-t+1}\sum\limits_{j=1-N+M}^{M} A^k(t-j+1)\cdot E_l^k(j), & \text{if} \quad N-M+2 \leqslant t \leqslant N \end{cases} \tag{8}$$

The original time series can be reconstructed, with no information loss, by summing all the RC as:

$$X_l(t) = \sum_{k=1}^{L\times M} R_l^k(t) \tag{9}$$

For filtering purposes, only the most correlated portion of the signal can be reconstructed by retaining only the $N_c$ first RCs. Note that, in that case, the choice of the number of RCs, $N_c$, must be done according to the eigenvalues values in order to retain most of the variance of the original signal.

In summary, M-SSA offers the possibility of analysing spatial and temporal correlations between different time series. The common modes of variability of the set of time series are described by empirical basic functions onto which each time series can be projected. Reconstructing time series using only a subset of these spatio-temporal modes offers the possibility to filter the signal by discarding the less correlated part of the signal. However, in order to perform M-SSA filtering, we first need to efficiently fill observational gaps in the time series (Figure 1). Here, we also take advantage of the M-SSA to perform temporal gap filling based on the information on the temporal structure of several time series.

### 3.2 Gap filling with M-SSA

We use a data-adaptative gap-filling algorithm based on single-channel SSA (Kondrashov & Ghil, 2006a,b; Kondrashov et al., 2010), and recently extended to M-SSA for GRACE and GRACE-FO applications (Prevost et al., 2019). To fill gaps in and between the GRACE and GRACE-FO observational periods, we take advantage of temporal correlations in the time series (F. Wang et al., 2020, 2021), to capture temporal modes of variability, and correlation between solutions processed by 4 different centres to limit processing artefacts (Prevost et al., 2019). Contrary to these recent studies, we perform gap filling on spatially distributed time series of Equivalent Water Height (EWH) rather than on their spherical harmonics equivalent (Prevost et al., 2019; F. Wang et al., 2021) in order to simplify the method overall by performing both gap filling and spatial filtering on time series of EWH. Consequently, we first convert Level-2 GRACE and GRACE-FO Stokes coefficients of the Earth's gravity field for each processing center $c$, at each date $t$, into global grids of surface mass anomaly $\sigma^c(t,\lambda,\varphi)$, where, $c \in$ [CSR, GFZ, GRAZ, JPL], $\lambda$ and $\varphi$ are the longitude and latitude. $\sigma^c(t,\lambda,\varphi)$ is expressed in EWH.

Our gap filling algorithm consists first in filling the observational gaps (Figure 1) for each point of geographic coordinates $(\lambda,\varphi)$ and each solution by performing a linear interpolation using data in the surrounding 50 months (centred on the data gap when possible). An example of linear interpolation of EWH is shown in Figure 4a for a point located in the Caspian sea (more examples are provided in Figure S1). Using a data window of 50 months rather than the entire time series for linear interpolation allows to capture potential regional or global variations in EWH trends (e.g.: large earthquakes signatures, changes in lake exploitation, acceleration of ice mass loss, etc.). For instance, the variation in trend in the Caspian sea, likely due to hydrological processes, between the artificially missing 2008 year, for method validation, and the 2017-2018 inter-mission period can be better recovered (Figure 4a). Here, we choose a linear interpolation over

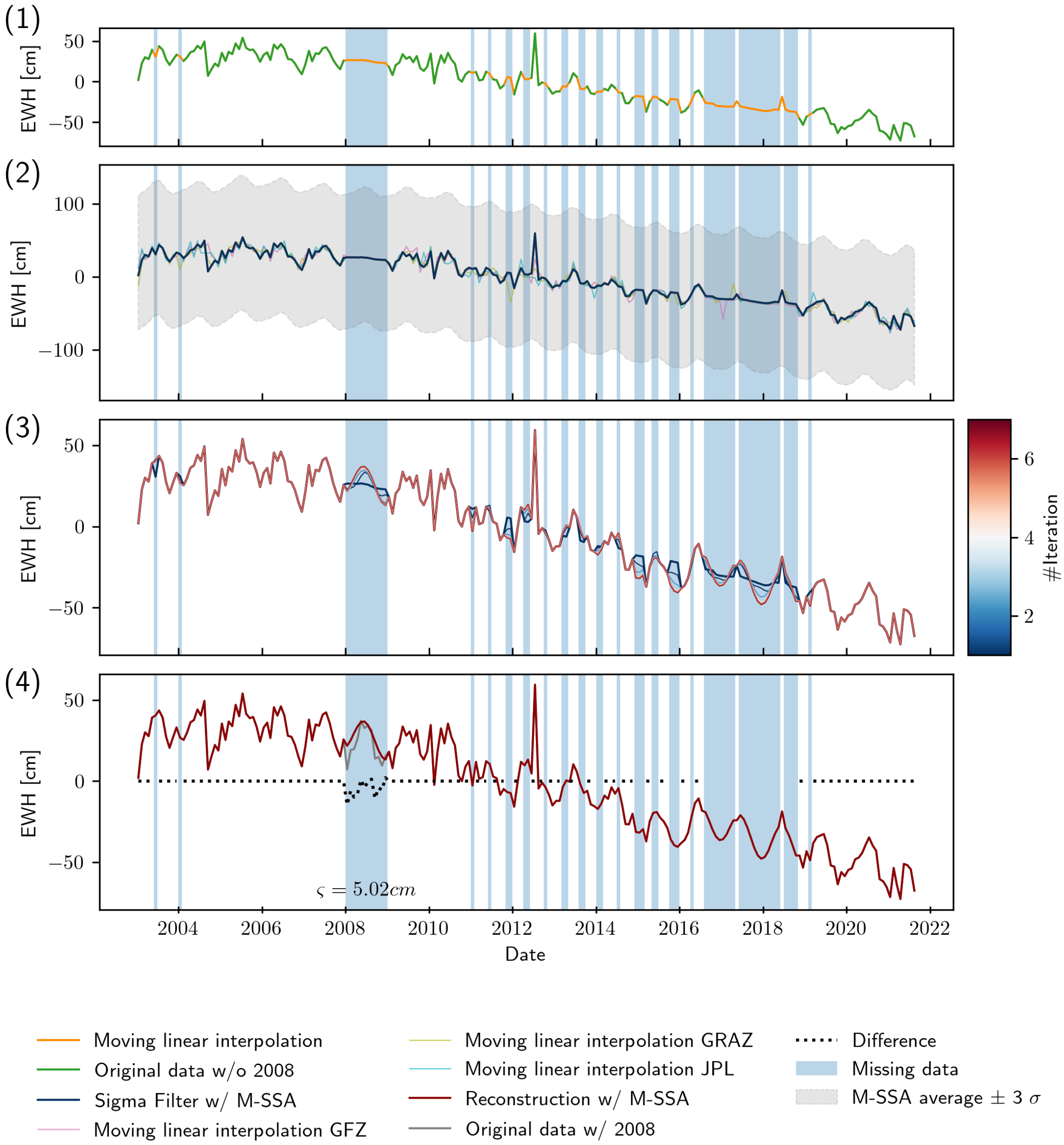


Figure 4: Example of M-SSA gap filling method for time series of CSR GRACE/GRACE-FO surface mass density anomalies, expressed in Equivalent Water Height (cm), for a point located in the Caspian Sea (51°E, 41°N). Observational gaps are highlighted in light blue. (a) shows the original EWH time series filtered by DDK7 and the Lobe-Edge filter (green, Lobe-Edge filter is presented in 3.4), and its evenly sampled version filled by a linear interpolation using a 50-month moving window (orange). (b) shows outliers identification, when they exists, based on a 3 times the standard deviation of a mean M-SSA based EWH time series of solutions processed by CSR, GFZ, GRAZ and JPL (orange, pink, khaki and cyan) criterion (light gray). Outliers are replaced by their mean M-SSA based EWH time series value to build a filtered version of the EWH time series (dark blue). (c) illustrates the iterative scheme to perform gap filling (blue to red). (d) Method performance is evaluated for year 2008, artificially removed from the original dataset and reconstructed, by comparing the final reconstruction (red) with the original GRACE observations (gray). Differences between the reconstructed and original signals for year 2008 are shown in dotted black line, and Root-Mean-Square value of the difference over 1 year is provided.

a mean or zero value gap filling to optimise M-SSA performances (Walwer et al., 2016; Prevost et al., 2019).

Once EWH times series are evenly spaced, thanks to the linear interpolation, it is possible to apply the M-SSA algorithm. However, because the reconstructed data gaps are highly influenced by the entire EWH time series, we first identify and replace outliers from EWH time series. For this purpose, we start by retrieving, for EWH time series of each point of coordinates ($\lambda$,$\varphi$), the principal modes of variability of the 4 solutions used in this study. To do so, we perform a M-SSA analysis on the 4 EWH time series simultaneously, using a sliding window of $M = N/2$, where $N = 224$ is the length of the evenly sampled GRACE/GRACE-FO time series for the period considered. We retain the first 8 PCs to reconstruct the signal for each solution, i.e. the first $N_c = 8$ RCs for each processing center $c$. A detailed analysis of M-SSA parameters selection is provided in the following for the gap filling method rather than the outliers detection, leading to similar results. We then average the reconstructed EWH time series of all processing centres to obtain a unique mean M-SSA-based EWH time series, $\sigma^m_{MSSA}(t, \lambda, \varphi)$, capturing the principal modes of variability of the signal processed by the 4 different centres. The average is defined as:

$$\sigma^m_{MSSA}(t, \lambda, \varphi) = \frac{1}{4} \sum_{c=1}^{4} \sum_{i=1}^{8} RC^i_l(t, \lambda, \varphi) \tag{10}$$

Finally, we identify outliers in EWH time series processed by individual centres as larger than three times the standard deviation of the mean M-SSA EWH time series, $\sigma^m_{MSSA}$ (see Figure S2 for tests on outliers detection criterion). Outliers, if they exists, are replaced by the corresponding value of $\sigma^m_{MSSA}$, while the rest of the time series remains identical for each processing center (Figure 4b and Figure S1 for additional examples).

Once outliers have been identified and replaced, we seek to improve the gap filling values, initially linearly interpolated, in the observational gaps. Therefore, we perform a M-SSA in an iterative scheme for each of the resulting 4 EWH times series simultaneously, corresponding to the 4 processing centres, filtered of their outliers and evenly spaced by linear interpolation. We use, once again, a sliding window of size $M = N/2$, half the length $N$ of the GRACE/GRACE-FO period considered. $M$ is chosen in order to capture the annual and long-term trends dominating the GRACE/GRACE-FO observations. To our knowledge, there is no optimal criterion to select $M$, but to provide separability of the series. Our value is chosen according to sensitivity tests summarised in Figure S3a. Data gaps are then iteratively replaced, in all solutions, by the sum of the first $N_c$ RCs resulting from the M-SSA on their combination. The value of $N_c$ is chosen based on Figure 5, which shows the box plots of normalised eigenvalues obtained from M-SSA analyses for all 4 centres for a selected subset of 3295 EWH time series encompassing a variety of signals of interests (see Figure S4 for location of the chosen EWH). Eigenvalues rapidly decrease until a noticeable drop after rank 8, with the first 8 EOFs capturing 73% of the original EWH time series variance, motivating the choice of $N_c = 8$ (see also Figure S3b for additional tests on parameter $N_c$). Note that adding EWH time series of nearby points at the same latitude in the M-SSA gap filling procedure has only little impact on the reconstruction and is therefore not considered (Figure S3c). Iterations are then performed until a convergence criterion, $\chi_c$, between the reconstructed signal at iteration $k$, $\sigma^c_k(t, \lambda, \varphi)$, associated with standard deviation $\varsigma(\sigma^c_k)$, and its previous iteration $k-1$ is reached. $\chi_c$ is defined, at iteration $k$, for $n$ missing observations, $n << N$, as:

$$\chi_c(\lambda, \varphi) = \sqrt{\frac{\sum_{t=1}^{n} \left(\sigma^c_{k-1}(t, \lambda, \varphi) - \sigma^c_k(t, \lambda, \varphi)\right)^2}{\varsigma(\sigma^c_{k-1}) \cdot \varsigma(\sigma^c_k)}} \tag{11}$$

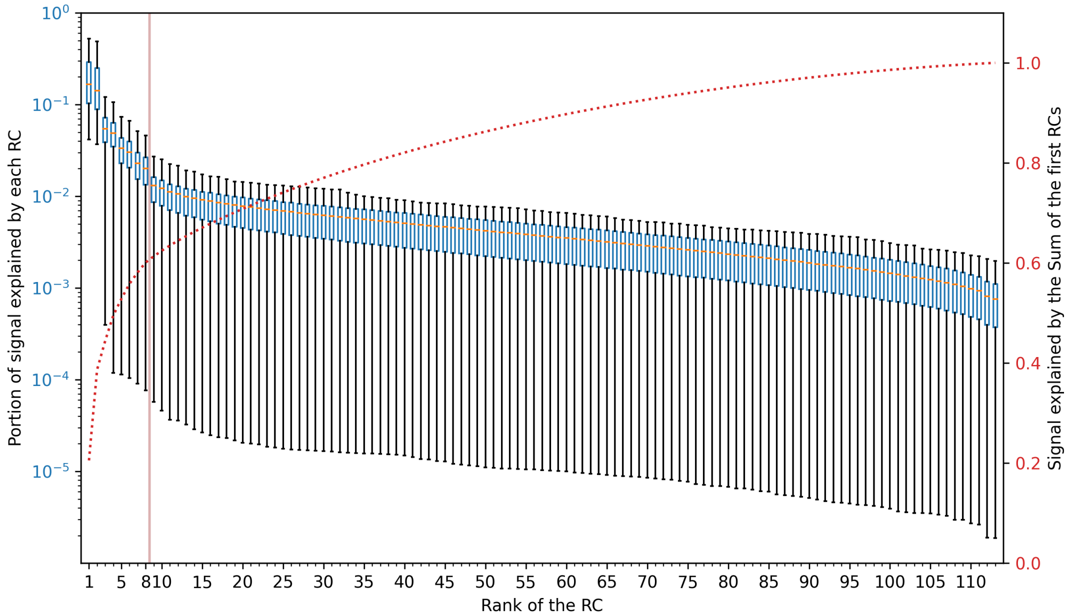


Figure 5: Normalised first 113 eigenvalues of the M-SSA analyses performed on a selected subset 3295 Equivalent Water Height (EWH) time series of the Level-2 GRACE and GRACE-FO gravity field processed by the CSR, GRAZ, GFZ and JPL centres simultaneously, after applying the DDK7 and Lobe-Edge filters and M-SSA gap fillings. Selected time series encompass a variety of signals of interest (see Figure S4 for a map of the chosen locations). The box plot shows the portion of the initial EWH time series variability explained by each Reconstructed Component (RC), according to its corresponding eigenvalue. The dotted red line shows the cumulative portion of the initial EWH time series explained by the sum of RCs. The red line highlights a drop in eigenvalues after rank 8, i.e. the limit of eigenvectors we used for signal reconstruction.

and satisfied for $\chi_c < 0.1$ or $n > 100$. Figure 4*c* shows an example, for a single processing center, of the successive signal reconstruction iterations until the convergence criterion, typically ranging between 7 and 16, is met (see Figure S1 for more examples).

The proposed gap filling method benefits from using solutions arising from 4 different processing centres by reconstructing observational gaps using only common signals retrieved by all solutions, thus limiting potential processing artefacts. In order to validate the method for filling the long 11-month gap between GRACE and GRACE-FO missions, we perform a synthetic test. Because modelling GRACE or GRACE-FO noise content is challenging due to its unknown exact structure, we artificially remove year 2008 of the GRACE dataset and test our gap filling method by reconstructing this missing year, in addition to existing missing dates. Figure 4d shows that the reconstruction for year 2008 of an EWH time series located in the Caspian Sea is consistent with the original signal, with differences between the original and reconstructed signals of the order of differences between different GRACE solutions (Figures 4d). The reconstructed time series captures particularly well the strong annual variations over the Caspian Sea, as well as the regional trend of decreasing mass. However only signals based on the statistical content of the entire time series can be reconstructed, discarding unusual events (ex: heavy rainfall, earthquakes, etc.). Additional examples are provided in Figure S1, and effects of the M-SSA parameters on the reconstruction of year 2008 are assessed in Figures S2 and S3. Once gaps in the EWH time series have been satisfyingly filled to obtain evenly sampled time series, spatio-temporal filtering using M-SSA can be performed.

### 3.3 M-SSA Spatial filtering

The second step of our method consists in performing a spatial filtering using the M-SSA to remove the remaining spatial noise. First, we average the 4 EWH time series obtained after gap filling, resulting from the 4 processing centres, into a single time series. Note that retaining or averaging these 4 EWH time series leads to similar M-SSA filtering results, but averaging them provides a computational advantage (Figure S5). Then, as we aim at removing residual spatially correlated noise, namely the spurious North-South stripes, we apply the M-SSA on the EWH time series at each point of the global $1^\circ \times 1^\circ$ grid and, simultaneously, and its 3 neighbouring EWH time series in both east and west directions, at the same latitude, spaced $2^\circ$ apart (Prevost et al., 2019). Thus, to filter a single EWH time series, 7 EWH time series are used. The number, distribution and distance between the neighbours of the reconstructed time series is defined by the spatial wavelength and shape of the spatially uncorrelated North-South stripes in order to extract only the correlated geophysical signals from the EWH time series through the M-SSA analysis. Parameters of the M-SSA for the spatial filtering step include a window size of $M = 13$ and a number of components for the reconstruction of $N_c = 8$. Note that $M$ for M-SSA filtering is significantly smaller than for gap filling since we are now more interested in retaining high frequency variations in the gravity fields rather than capturing its main features for reconstruction. Sensitivity tests on M-SSA filtering parameters $M$, $N_c$, number and distance of neighbouring EWH time series are provided in Figure S6. Note that $N_c$ is defined similarly to the M-SSA reconstruction method, but now based on the eigenvalues of the M-SSA analysis of a EWH time series and its neighbouring time series (see Figure S7).

For example, Figure 6 shows the M-SSA decomposition of the CSR EWH time series obtained after gap filling, for a point located in the Caspian Sea. The first 8 RCs show the potential of the method to separate and retrieve the dominant long term variation of the Caspian Sea (RC 1), strong annual (RC2, RC3, RC5) and semi-annual (RC6) variations as well as multi-annual variations (RC4). In fact, most of the variance of the filtered and evenly sampled EWH time series can be explained by the first 8 components as shown by Figure 6f. The final EWH time series, after both the gap filling and spatial filtering steps of the method is shown on 6a, and compared to the gap filling step and the initial DDK7-filtered time series. The method efficiently removes high frequency noise, unlikely related to changes in the Caspian sea level as supported by satellite altimetry measurements (J. Chen et al., 2017). Other examples of locations are provided in Figure S8.

### 3.4 Complementary filtering in the spherical harmonics domain: Lobe-Edge filter

In order to refine a first DDK7 M-SSA solution, we have designed an additional filter to reduce the remaining lobes of spurious errors detected, down to the amplitude level observed for lower orders, and same degree of the spherical harmonics decomposition (Figure 7a). This filter has been applied after the decorrelation filter, here DDK7, and before the M-SSA gap filling and filtering procedures. To build the filter, we used the average GRACE/GRACE-FO surface mass density anomalies, after an initial DDK7 filtering, M-SSA gap filling and spatial filtering, and once dominant geophysical signals have been removed using parametric functions. A degree-3 polynomial function, representing linear trends and multi-annual signals, is removed while dominant seasonal signals are subtracting the monthly averaged throughout the observational period from each monthly solution. Residuals are expressed in terms of Stokes coefficients $X^r_{l,m}$, which is the mean value of $C^r_{l,m}$ and $S^r_{l,m}$, for a given degree $l$ and order $m$. We define the Lobe-

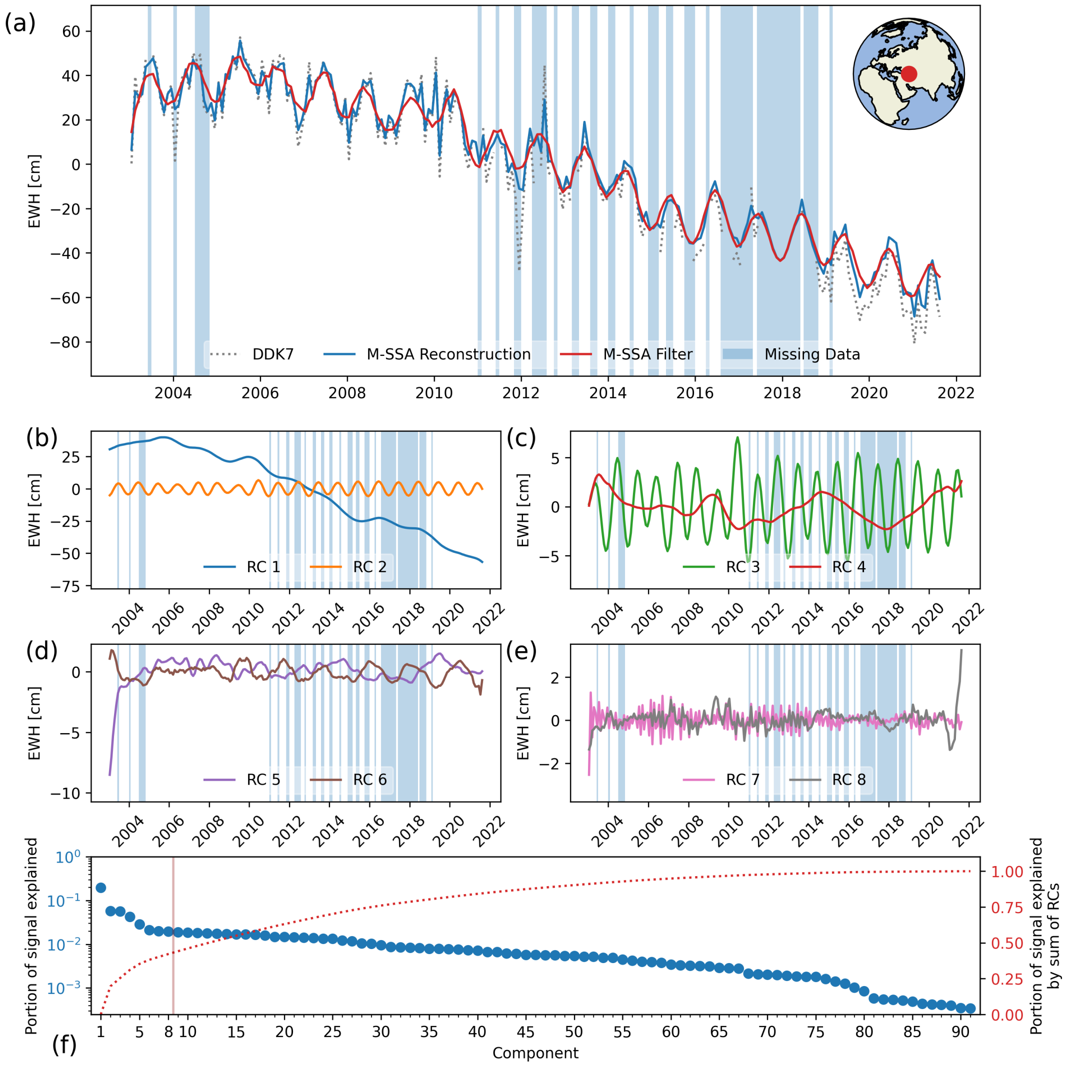


Figure 6: M-SSA spatio-temporal decomposition of the surface mass density anomalies for a point located in the Caspian Sea (51°E, 41°N). Time series (a) shows the final CSR Equivalent Water Height (EWH) time series, after the DDK7 and Lobe-Edge filtering (Lobe-Edge filter, presented in Section 3.4, further reduces striping noise) , M-SSA gap filling, using information from 4 processing centres, and spatial filtering, using an EWH time series and its neighbours located at the same latitude (red), compared to the gap filling procedure only (blue), and the initial DDK7-filtered (dotted gray) time series. (b)-(f) display the first 8 RCs of the decomposition, sorted by their corresponding eigenvalue. (g) shows the normalised eigenvalues obtained from the M-SSA spatial filtering.

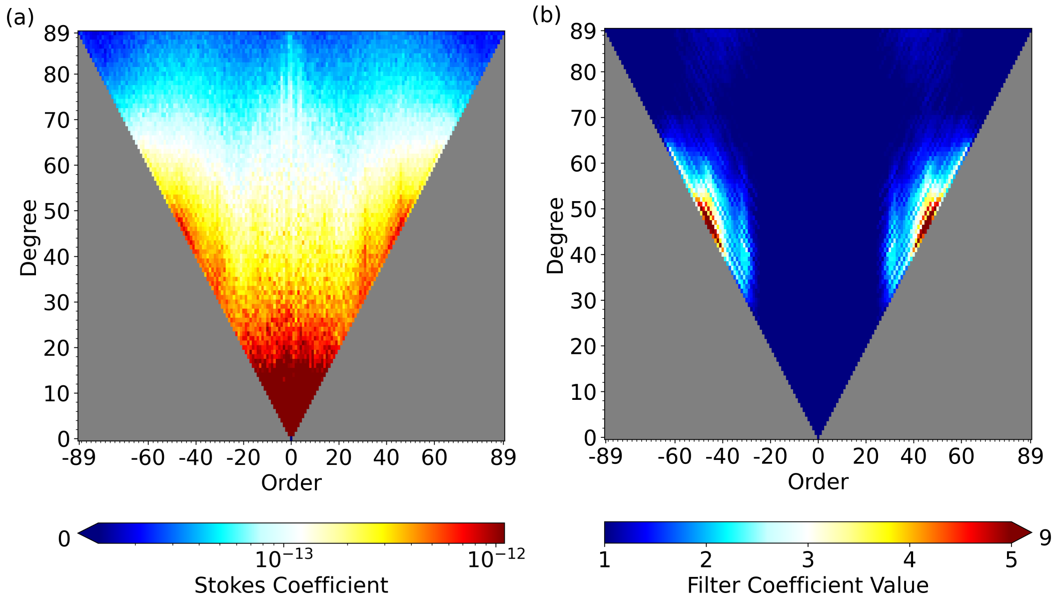


Figure 7: (a) Intensity spectrum of Stokes coefficients of the average of GRACE/GRACE-FO monthly surface mass density anomaly, after DDK7 and M-SSA gap filling and spatial filtering, and once dominant geophysical signals have been removed using parametric functions. These signals include a degree-3 polynomial function, reflecting linear trends and multi-annual signals. Dominant seasonal signals are accounted for by removing from each monthly solution, its monthly averaged over the observational period. (b) Intensity spectrum of the Lobe-Edge coefficients designed based on (a) and Equation 12, for $\alpha = 1.5$.

Edge (LE) filter, for which each coefficient, $F^{LE}_{l,m}$, for a given exponent $\alpha$ is :

$$\begin{cases} F^{LE}_{l,m} = \left( \dfrac{\frac{1}{6} \cdot \sum\limits_{n=-1}^{1} abs(X^r_{l-n,m-n} + X^r_{l-n,n-m})}{\frac{1}{41} \cdot \sum\limits_{n=-20}^{20} X^r_{l,n}} \right)^{\alpha} & \text{for} \quad F_{l,m} \geq 1, \quad l \geq 25, \quad m \geq 25 \\ F^{LE}_{l,m} = 1 & \text{otherwise.} \end{cases} \tag{12}$$

By averaging the residual signal $X^r_{l,m}$, for $l \geq 25, m \geq 25$ and dividing its amplitude by the mean amplitude of $X^r_{l,m}, -20 \leq m \leq 20$, we design a filter that is adapted to dampen the amplitude of the lobes of residual signal detected. Value of exponent $\alpha$, here equal to 1.5, is chosen to ensure that the signal amplitude in the lobes for a given degree $l$, after Lobe-Edge filter has been applied, is comparable to its value over all orders $m$. Outside of the lobes, no additional filtering is performed. Coefficients of the Lobe-Edge filter are shown on Figure 7b (see Figure S9 for Lobe-Edge filters coefficients for various values of $alpha$). By design, coefficients of order $-20 \leq m \leq 20$ are not impacted by lobe-edge filtering, whereas coefficients of degrees $l$=40 to 50 and orders $m \geq 25$ can reach values up to 5 to efficiently filter persistent non-physical noise detected by our approach.

The LE filter is applied to monthly GRACE and GRACE-FO solutions $X_{l,m}$, after DDK7 filtering, as:

$$X^{LE}_{l,m} = \frac{X_{l,m}}{F^{LE}_{l,m}} \tag{13}$$

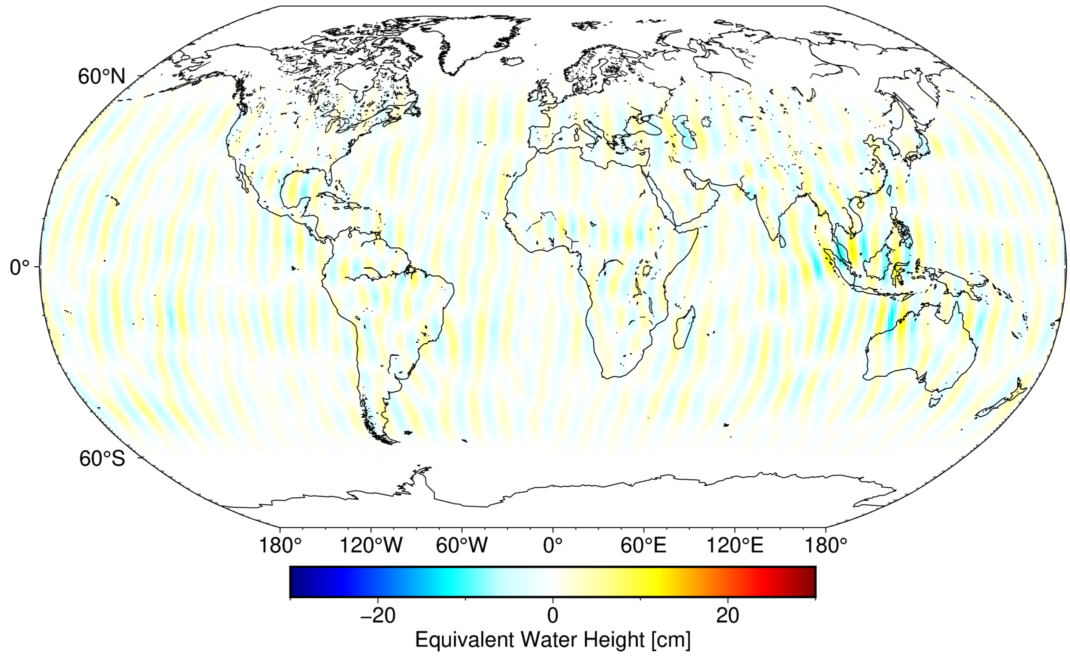


Figure 8: Map of the differences between the combined DDK7 + Lobe-Edge, with filter exponent $\alpha = 1.5$, and DDK7 only filtered GRACE-FO July 2019 monthly solutions, expressed in Equivalent Water Height.

Figure 8 shows an example of the impact of applying the additional LE filter to the DDK7-filtered GRACE-FO July 2019 monthly solution in the spatial domain. LE filtering efficiently removes spurious North-South stripes with significant amplitude, reaching up to $\sim$10 cm. In fact, the amplitude of North-South stripes removal is determined by the choice of LE filter exponent parameter $\alpha$ and lies in a compromise between efficiently filtering noise and preserving signals of geophysical origin. In particular, we notice that the stripes amplitude is higher in the region affected by the 2004 Mw 9.1 Sumatra-Andaman earthquake (Figure 8), indicating that the LE filter could possibly absorbing part of the gravity signals resulting from the regional seismic cycle. However, the gain in removing noise is larger than the loss of signal improving the global signal to noise ratio. Examples of results for other values of $\alpha$ are provided in Figures S10 for July 2019, and a particular attention is given to the 2004 Mw 9.1 Sumatra-Adaman earthquake region (Figure S11).

However, overall, the LE filter proves efficient at removing residual North-South striping noise, after DDK filtering. We therefore include the LE filter in our GRACE/GRACE-FO post-processing strategy, after applying DDK7 and prior to perform M-SSA gap filling and filtering procedures. Figure 9 shows an example of the effect of adding LE filtering to our post-processing strategy on final EWH time series for a point located in the Caspian sea. LE filtering helps removing part of the residual high frequency noise in the Caspian sea EWH time series. Examples of the full M-SSA spatio-temporal decomposition, after DDK7 and LE filtering, M-SSA gap filling and spatial filtering, are provided in Figure S12. Our final GRACE/GRACE-FO M-SSA solution, for which results are presented and discussed in following, is therefore a combination of DDK7 and LE filtering, with M-SSA gap filling and local filtering.

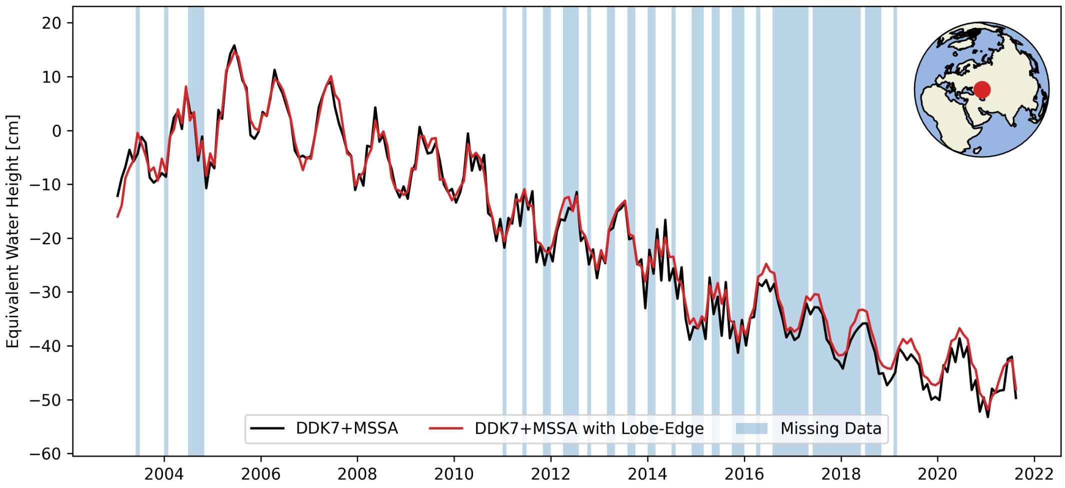


Figure 9: Comparison of GRACE/GRACE-FO Equivalent Water Height (EWH) time series after DDK7 filtering, M-SSA gap filling and spatial filtering (black) or DDK7 and Lobe-Edge filtering, M-SSA gap filling and spatial filtering (red) for a point located in the Caspian Sea (51°E, 46°N).

### 3.5 Results

We compare our final GRACE/GRACE-FO M-SSA solution with two other solutions in spherical harmonics (SH), all corrected for Glacial Isostatic Adjustment contributions using the ICE-6G model (Argus et al., 2014; Peltier et al., 2015, 2018). The first one is the average of SH solutions processed by CSR, GRAZ, GFZ and JPL, filtered using DDK5, which is recommended and commonly used for geophysical applications (Sakumura et al., 2014). The second one uses DDK7, which is the initial filtering of the GRACE and GRACE-FO gravity fields before Lobe-Edge filtering, M-SSA gap filling and filtering procedures developed in this study.

Figure 10 shows maps of the GRACE EWH for the month of July 2007, relative to January 2007, for all three solutions, after removing the linear trend estimated over the 2003-2021 period. Differences between gravity fields, which highlight the noise content of solutions, proves the efficiency of the method proposed in this study to remove characteristic nonphysical North-South striping patterns in the GRACE gravity fields. While both the DDK5 (Figure 10a) and DDK7 (Figure 10b) filtered 2007 GRACE July-January solutions display persisting stripes, particularly visible in the oceans, the final M-SSA solution (Figure 10c) shows only negligible striping patterns. Moreover, compared with the recommended solution for geophysical applications (Sakumura et al., 2014), the final M-SSA solution is initially filtered using DDK7 rather than DDK5, which further attenuates signals and smears them out signals over larger regions. While a simple DDK7 filtering of the gravity fields may retain smaller spatial wavelengths signals, the high noise content of the resulting solutions prevents geophysical interpretations (Figure 10b). Since the final GRACE-MSSA is initially filtered using DDK7, in combination with an objective filtering approach through M-SSA, it successfully retains a higher spatial resolution than DDK5-filtered solutions, while removing sufficient North-South stripes to allow for geophysical interpretation. For example, the gravity signature of seasonal variations in surface and groundwater in the Lena basin in west part of Russia or Mississippi river basin in Central United States (J. Chen et al., 2007; Rodell et al., 2007; Larochelle et al., 2022) appears spatially more focused in the M-SSA GRACE solution than in the DDK5 averaged solution, and is undetectable in the DDK7 averaged solution.

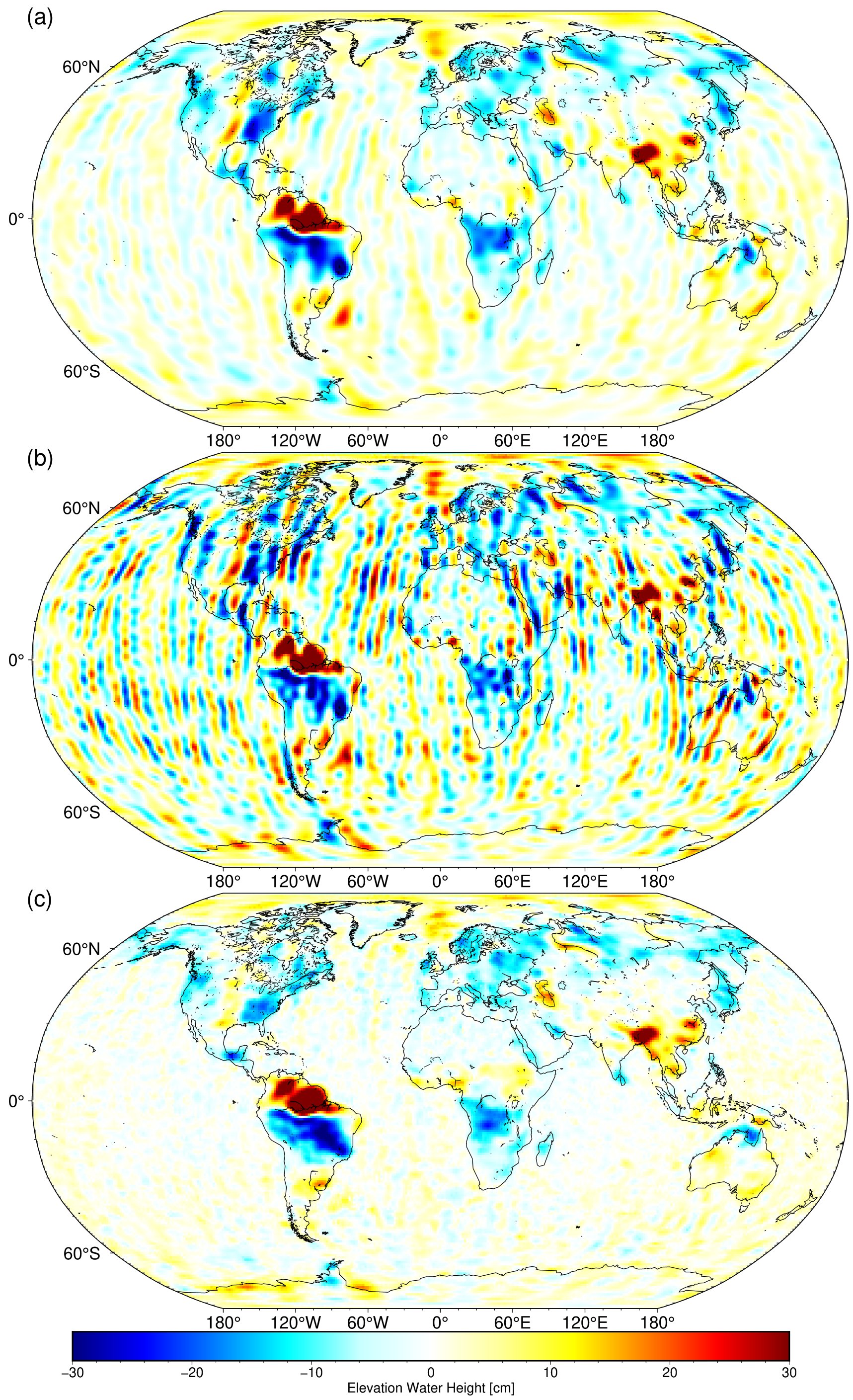


Figure 10: GRACE surface mass density anomaly for the month of July 2007, relative to January 2007, expressed in Equivalent Water Height, corrected for Glacial Isostatic Adjustment contributions (ICE-6G, Peltier et al. (2018)) for the average of CSR, GFZ, GRAZ and JPL solutions after applying (a) DDK5 filter, (b) DDK7 filter, and (c) the final GRACE M-SSA solution presented in this study.

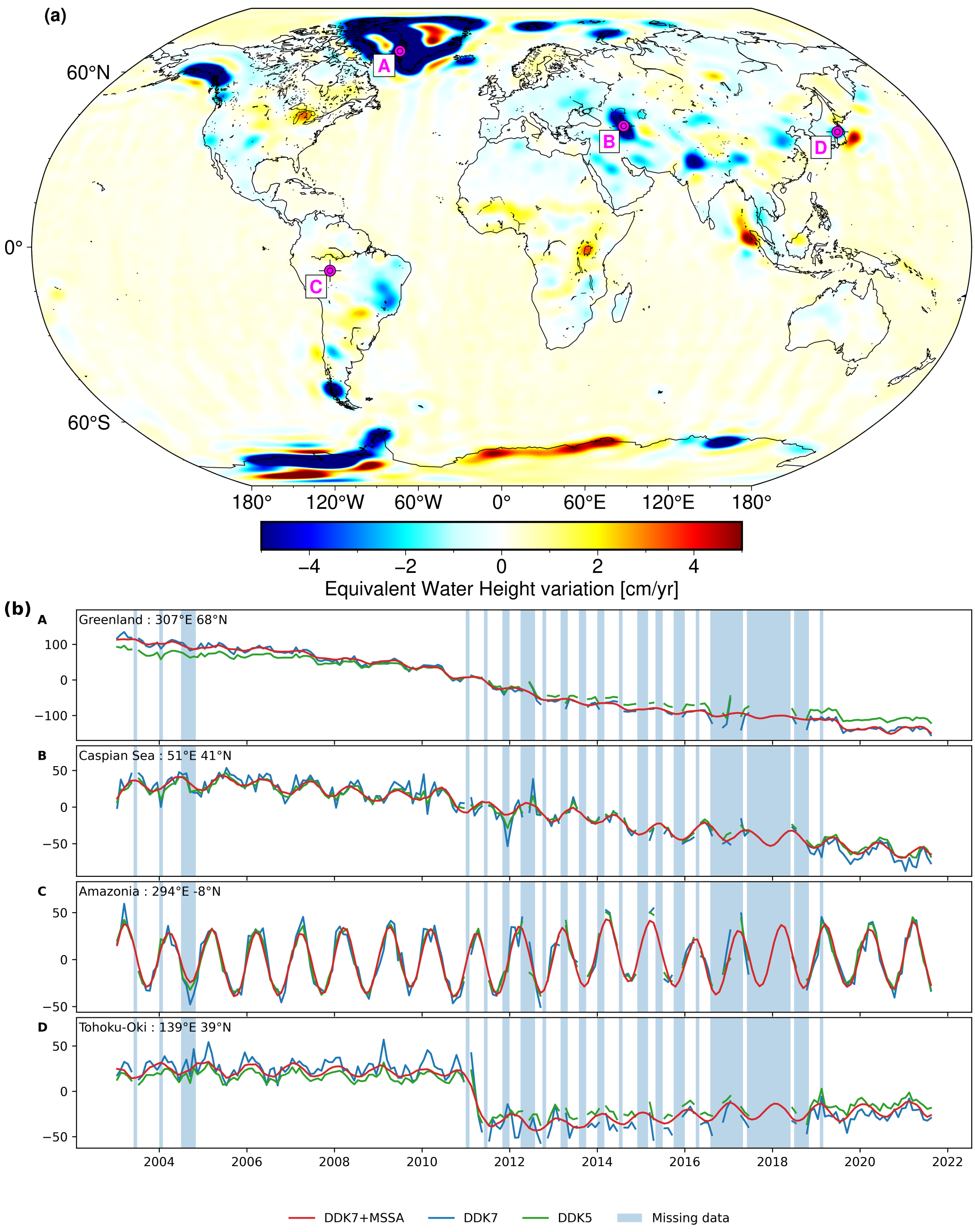


Figure 11: (a) Mean rate of surface mass density anomaly of the final GRACE M-SSA solution presented in this study, from January 2003 to December 2021, expressed in Equivalent Water Height (EWH) per year. (b) Comparisons of EWH time series at points located in Greenland, the Caspian sea, the Amazonian basin and in the region of the 2011 Mw 9.1 Tohoku-Oki earthquake, pointed out on (a). EWH are shown for the average of CSR, GFZ, GRAZ and JPL solutions after applying DDK5 filter (green), DDK7 filter (blue), and the final GRACE M-SSA solution presented in this study (red).

Figure 11a shows the mean rate of surface mass density anomaly of the final GRACE M-SSA solution, from January 2003 to December 2021. While the noise content of the GRACE M-SSA trend solution reaches a level comparable to the trend of the average of CSR, GFZ, GRAZ and JPL solutions filtered by DDK5, its spatial resolution, and therefore signal attenuation, is comparable to the DDK7-filtered one (Figure S13). Indeed, while major large scale long-term evolving phenomena, such as recent ice-sheets melting (ex: Greenland) or large variations in continental hydrology (ex: Caspian sea), are seen in all solutions, smaller spatial scales features consistent with regional geophysical processes are visible in the GRACE M-SSA solution including smaller magnitude earthquakes (ex: 2009 Mw 8.0 Samoa outer-rise earthquake) or smaller glaciers ice mass loss (ex: South Georgia) (Prevost et al., 2019). Consequently, long-term trends between the commonly used average of CSR, GFZ, GRAZ and JPL solutions filtered by DDK5 and the GRACE M-SSA solution may locally differ. For example, Figure 11b shows comparisons of EWH times series for all solutions at a selected set of locations. While trends may agree in hydrological basins where mass variations occur at large scale such as the Amazonian basin, they tend to disagree in regions with more heterogeneity including for example Greenland coastal area and the Caspian sea, potentially leading to an improvement in regional mass balance such as in Greenland using solutions with a higher spatial resolution. Unfortunately, the GRACE M-SSA solution does not retrieve abrupt mass change related for example, to the co-seismic gravity signal of the 2011 Mw 9.1 Tohoku-Oki earthquake, as well average of CSR, GFZ, GRAZ and JPL solutions filtered by DDK7. This is due to temporal filtering associated with the M-SSA method. A specific processing over regions affected by large earthquakes would be required to improve the final GRACE-M-SSA solution but is beyond the scope of this study.

Overall, the GRACE/GRACE-FO M-SSA solution, including DDK7, LE filtering, M-SSA gap filling and spatio-temporal filtering, efficiently removes characteristic North-South striping pattern, while retaining a higher spatial resolution than the widely used average of gravity fields SH solutions filtered by DDK5. Main features in trend and annual variability of the final GRACE/GRACE-FO M-SSA time series are comparable to those of DDK7 filtered gravity fields, consistent with the rest of the time series over reconstructed missing observations, and show a significantly lower noise content. In the following Section, we attempt at assessing the GRACE/GRACE-FO M-SSA solution through comparisons with independent observations and GRACE/GRACE-FO processing techniques.

# 4 Discussion

We now focus on verifying consistency between our final GRACE/GRACE-FO M-SSA solution and independent datasets, including observations, models and different GRACE/GRACE-FO processing strategies, to assess the quality of both gap filling and spatio-temporal filtering at the global and local scale using the method developed in this study.

## 4.1 Global scale comparisons

### *4.1.1 Gap filling validation for low spherical harmonics gravity field coefficients: a comparison with SLR data*

We first seek to compare the final GRACE M-SSA solution with Satellite Laser Ranging (SLR) observations. SLR orbits are determined through the measure of the round trip time of a laser beam between satellites and ground tracking stations. Due to their spherical geometry and favorable area-to-mass ratio limiting a number of sources of uncertainties, SLR satellites are optimal for deriving accurate information on the Earth's gravity field. Unfortunately, due to the limited distribution of ground tracking stations, SLR only gives access to temporal variations of the low spherical harmonic degrees of the gravity field (Sośnica et al., 2015).

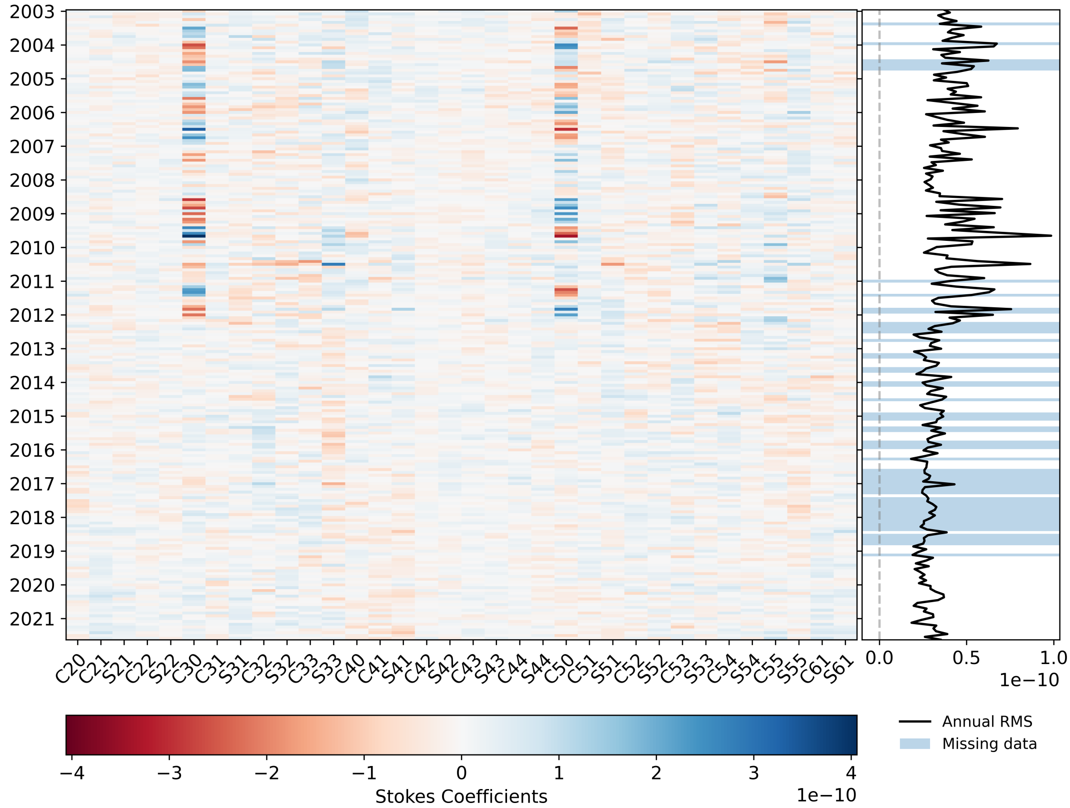


Figure 12: Time dependent Root Mean Square Deviation (RMSD) of the difference between low degree Stokes coefficients of the GRACE M-SSA solution and CSR SLR estimates (left), and a time series of their cumulative variation over the 2003-2021 period (right). Coefficients $C_{2,0}$ and $C_{3,0}$ have been replaced according to the Technical Note 14 (TN-14; J. Chen et al. (2005); Loomis et al. (2020)), starting in January 2003 and March 2012 respectively. GRACE and GRACE-FO observational gaps, reconstructed using the M-SSA approach proposed in this study, are highlighted in blue.

Thus, here we compare the final GRACE/GRACE-FO M-SSA solution with the SLR Stokes coefficients of the gravity field provided by CSR up to the degree 6 order 1 (excepted the degree 6 order 0) (Cheng et al., 2011). Figure 12 shows variations in the Root Mean Square Deviation (RMSD) of the difference between low degree Stokes coefficients of the GRACE/GRACE-FO M-SSA solution and CSR SLR estimates, and a time series of their cumulative variation over the 2003-2021 period. As a reminder, we have replaced the $C_{2,0}$ and $C_{3,0}$ coefficients, starting in January 2003 and March 2012 respectively, according to the Technical Note 14 (TN-14; J. Chen et al. (2005); Loomis et al. (2020)). RMSD between our final GRACE/GRACE-FO M-SSA solution and SLR-derived Stokes coefficients are negligible except for $C_{3,0}$ and $C_{5,0}$ over the January 2003-February 2012 period. We attribute the abnormal high amplitude of $C_{3,0}$ prior to February 2012 to its replacement recommendation only after March 2012 and suggest that it is extended to the entire time series. Established anti-correlated resonance between $C_{3,0}$ and $C_{5,0}$ may explain the large discrepancies between the GRACE M-SSA and SLR solutions for $C_{5,0}$ before March 2012 (Sośnica et al., 2015; Loomis et al., 2020). As a result, the annual mean amplitude of the RMSD between GRACE/GRACE-FO M-SSA and SLR Stokes coefficients (Figure 12) decreases after March 2012 and more interestingly, remains at similar level during observational gaps filled by the method proposed in this study. This suggests that observational gaps filled by M-SSA are comparable to independent SLR observations for low degree Stokes coefficients. Existing GRACE and GRACE-FO observations for low degree Stokes coefficients, which are unlikely impacted by our post-processing filtering approach, remain consistent with SLR observations throughout the entire time series.

#### *4.1.2 Comparison with hydrological model*

We now want to assess performances of our final GRACE M-SSA solution gap filling method with an independent dataset of higher spatial resolution. Since a large portion of the gravity field variations recorded by GRACE/GRACE-FO signal are driven by continental hydrology (Syed et al., 2008), GRACE solutions are commonly compared to independent estimates of variations in land hydrology such as the Global Land Data Assimilation System (GLDAS) (Longuevergne et al., 2013). GLDAS provides estimates of land surface hydrology based on satellite and in-situ observations, combined with advanced land surface modelling and data assimilation techniques (Rodell et al., 2004). In particular, GLDAS provides 1° x 1° grids of estimated variations in snow, canopy water and soil water components between the surface and 2 meters depth but not deeper

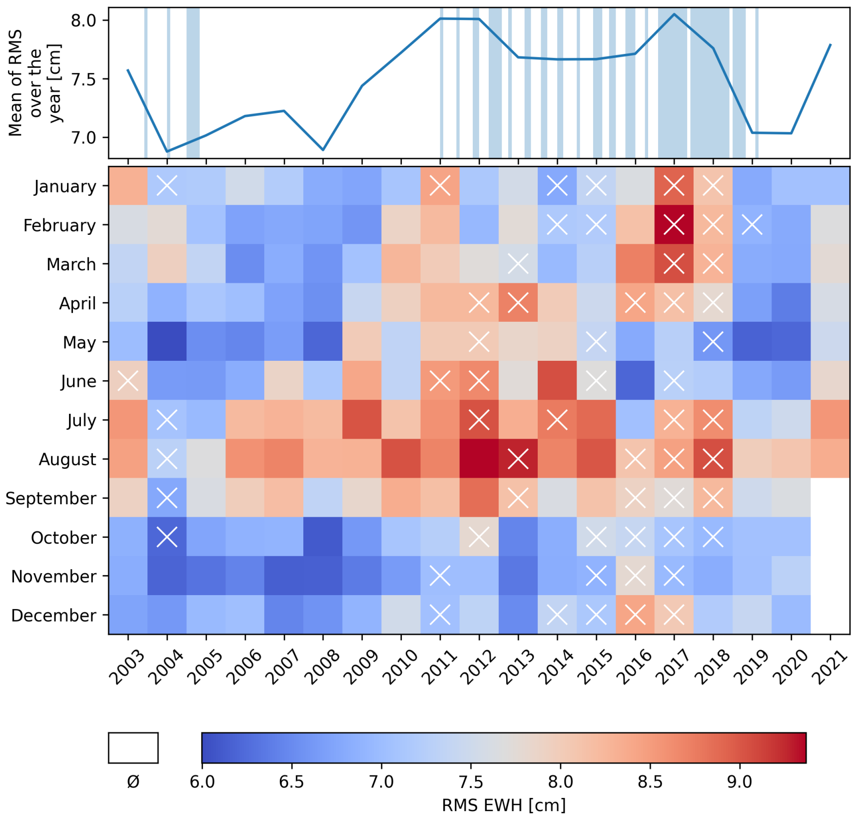


Figure 13: Root Mean Square Deviation (RMSD) over continental areas between the final GRACE/GRACE-FO M-SSA solution and the Global Land Data Assimilation System (GLDAS) (Rodell et al., 2004), expressed in Equivalent Water Height (EWH). Yearly averaged RMSD (top) and monthly RMSD (bottom) are shown over the 2003-2021 period. Missing periods of GRACE/GRACE-FO observations, reconstructed using the M-SSA procedure proposed in this study are highlighted in light blue (top) and white crosses (bottom).

groundwater. We convert the GLDAS datasets into EWH, sum, and compare to the final GRACE/GRACE-FO M-SSA solution.

Figure 13 shows the RMSD between GRACE/GRACE-FO M-SSA and GLDAS averaged over continental areas. Significant discrepancies, reaching up to 10 cm of EWH on global continental average, occur during the summer months, likely due to the absence of groundwater and ice components in GLDAS that bear large seasonal variations. Reconstructed months, through the M-SSA gap filling procedure, tend to reflect this feature, particularly during the 11-month gap between missions. Note that during this period, and toward the erratic end of the GRACE mission, GRACE/GRACE-FO M-SSA reconstructions also show large discrepancies with GLDAS from January to April, which are not annually recurrent, but do reach similar values in 2010 and 2011. In fact, the yearly RMSD between the final GRACE/GRACE-FO M-SSA solution and GLDAS, averaged over continental areas shows comparable values over the entire 2003-2021 time series, including M-SSA filled GRACE observational missing periods. While we do not argue that statistically reconstructed GRACE observations over missing months should be geophysically interpreted, the final GRACE/GRACE-FO solution offers a continuous record of gravity field variations, that can help, for example, recovering the long-term evolution of some processes (earthquake cycle, GIA, recent ice melting, water depletion, etc.).

The gap filling procedure used to process the GRACE/GRACE-FO M-SSA is consistent, to first order, with independent observations including low degree Stokes coefficients derived from SLR and estimations of variations in land hydrology. We now seek to compare the quality of the GRACE/GRACE-FO M-SSA with other GRACE/GRACE-FO solutions to assess the potential of our final solution to efficiently remove North-South stripes while retaining smaller spatial wavelength geophysical signals.

#### *4.1.3 Comparison with other GRACE/GRACE-FO solutions*

A metric commonly used to quantify noise level in GRACE and GRACE-FO solutions is to compute the Root-Mean-Square (RMS) value over the ocean (Bonin et al., 2012; Meyer et al., 2016). Since gravity fields have been corrected for non-tidal high-frequency atmospheric and oceanic mass variation models (AOD1B; Dobslaw et al. (2017)), signal over the ocean should be small, and dominated by remaining random errors. To further reduce any signal of geophysical origin, we first fit and remove a degree-3 polynomial, annual and semi-annual sine functions to EWH time series at each point of a global $1^\circ \times 1^\circ$ grid. This functions account for potential geophysical signals in the GRACE and GRACE-FO over the oceans, including leakage signals in coastal areas related to continental mass smeared out over large regions due to the missions intrinsic spatial resolution and filtering approach. Note that we exclude regions of major earthquakes, by removing oceanic areas of observations around epicenters which size is determined based on the GRACE/GRACE-FO M-SSA mean rate of surface density anomaly. Earthquakes considered are the 2004 Mw 8.8 Sumatra-Andaman, 2010 Mw 9.1 Maule and 2011 Mw 9.1 Tohoku-Oki eartquakes. Finally, we exclude latitudes above 45° and below -45°, where non-tidal ocean signals are more challenging to predict. Figure S14 shows a map of the ocean region considered used to compute RMS. Figure 14a shows consistent low noise level of the final GRACE/GRACE-FO M-SSA solution, with EWH values remaining below $\sim$1 cm. To compare performances with other solutions, we also compute the RMS over the ocean of the difference between the final GRACE/GRACE-FO M-SSA solution and the average of DDK7-filtered SH CSR, GFZ, GRAZ and JPL solutions, the DDK5-filtered COST-G combination solution (Meyer et al., 2019; Jäggi et al., 2020) and the CSR mascons independent processing strategy . Absolute RMS values over the oceans for all solutions are shown in Figure S16. The GRACE/GRACE-FO M-SSA solution efficiently removes noise compared to DDK7-filtered solutions, which are the starting point of the method (Figure 14b), and contain lower noise level than the combined COST-G even if it is filtered at a higher level, using DDK5 (Figure 14c). More importantly, the

GRACE/GRACE-FO M-SSA solution noise level over the ocean reaches the CSR mascons noise level, which is low by construction due to strong regularisation in oceans, but with no *a priori* constraints or regularisation on the noise or signal distribution (Figure 14d). Comparison with the average of DDK5-filtered SH CSR, GFZ, GRAZ and JPL solutions and JPL mascons solution yield similar conclusions (Figure S15).

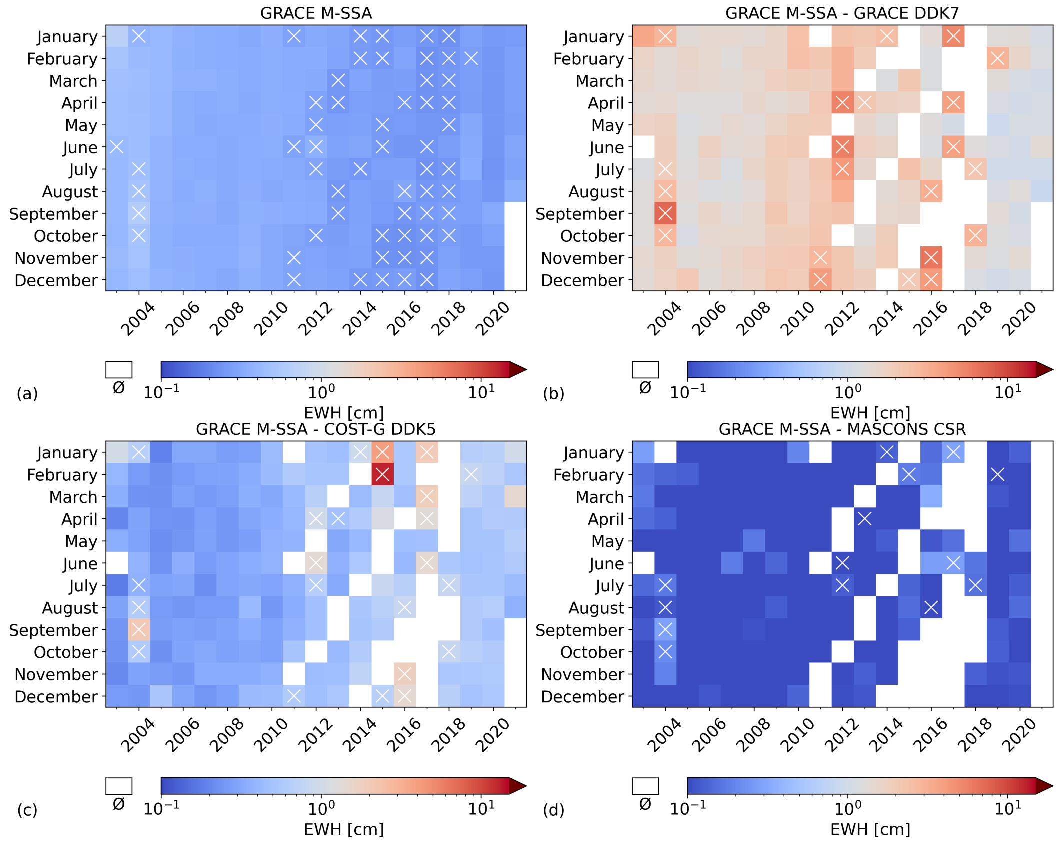


Figure 14: (a) Root-Mean-Square (RMS) value of the final GRACE/GRACE-FO M-SSA solution over the ocean, expressed in terms of Equivalent Water Height (EWH), after fitting and removing a degree-3 polynomial, annual and semi-annual sine functions from EWH time series at each point of a global 1° × 1° grid. This functions account for potential signals of geophysical or leakage origin in the ocean. Regions of large earthquakes and latitudes below and above 45° are excluded from the RMS computation (see Figure S14 for a map of the region considered). RMS of the difference between the final GRACE/GRACE-FO M-SSA solution and (a) the average of DDK7-filtered CSR, GFZ, GRAZ and JPL solutions, (b) the DDK5-filtered COST-G combination solution and (c) the CSR mascons independent processing strategy.

Overall, the M-SSA based gap filling and filtering methods lead to a final GRACE/GRACE-FO M-SSA solution that is consitent with independent datasets and contains a lower noise level than the other SH solutions presented here, independently of the choice of a DDK7 or DDK5 filter. However, any filtering of the GRACE/GRACE-FO gravity fields generated from SH Stokes coefficients necessarily causes signal attenuation and leakage. Thus, at the local and regional scales, we compare the final GRACE/GRACE-FO solution, as well as other SH solutions, with the independent mascons processing technique.

## 4.2 Local and regional scale comparisons

### *4.2.1 Comparisons of Equivalent Water Height time series*

We compare EWH time series at a selected set of locations in regions of geophysical interest (Figure 15). On one hand, the overall features retrieved with the GRACE/GRACE-FO M-SSA solution agree with all SH solutions, despite discrepancies in the higher frequency content of the time series, likely due to the noise content of each solution. In particular, the method proposed in this study agrees well with the initial method proposed by Prevost et al. (2019), with a larger portion of the North-South stripes removed thanks to the Lobe-Edge filter, and a simplified processing with M-SSA applied on EWH only. On the other hand, major differences between SH solutions and the CSR mascons solution appear. First, for a point located on the western central coast of Greenland (Figure 15a), the rate of surface mass density loss is surprisingly twice larger for the CSR mascons solution than for SH solutions, all corrected for GIA contribution, in a region that is not covered by ice and thus where no mass variation related to recent ice melting is expected. Furthermore, for a point located in the region of the 2011 Mw 9.1 Tohoku-Oki earthquake (Figure 15b), the co-seismic gravity signal is 4 times larger in the CSR mascons than in the SH solutions, driven by the parametrization of the regularisation matrix used to develop the mascons solution (Save et al., 2012, 2016). Such differences raise the question of GRACE and GRACE-FO mass variations validation to ground truth independent measurements to quantitatively assess solutions performances.

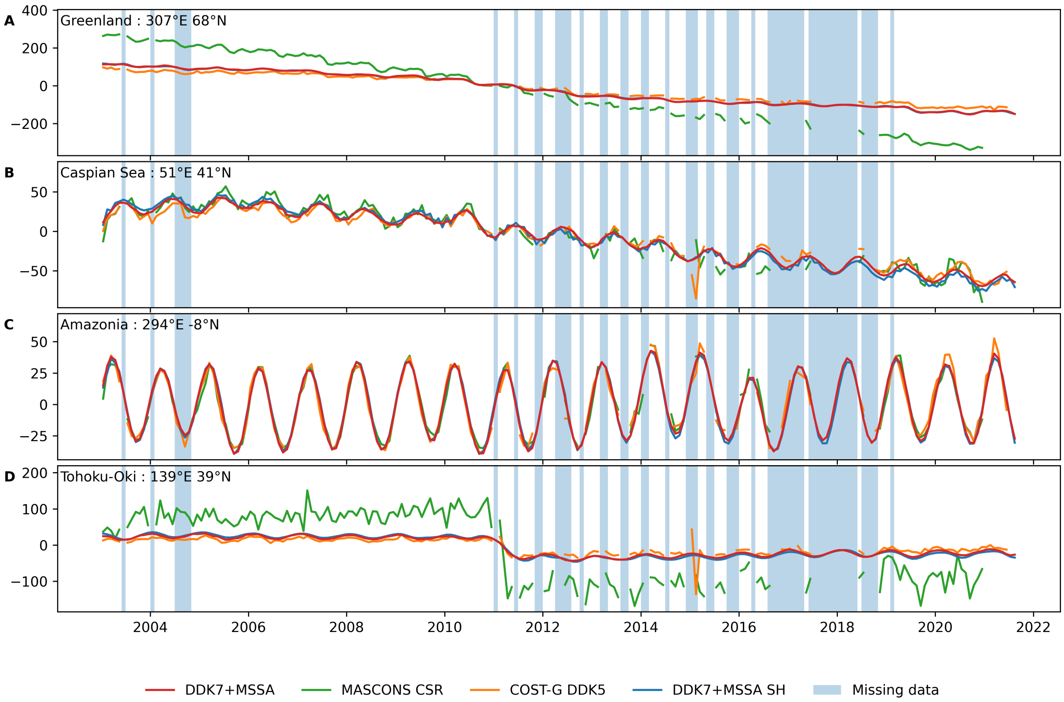


Figure 15: Time series of surface mass density anomaly, expressed in Equivalent Water Height (EWH), at points located in Greenland, in the Caspian sea, in the Amazonian basin and in the region of the 2011 Mw 9.1 Tohoku-Oki earthquake (see location map on Figure 11). EWH times series are compared for 4 different solutions: the final GRACE/GRACE-FO M-SSA solution presented in this study (red), the GRACE/GRACE-FO M-SSA solution based on Prevost et al. (2019) (blue), the combined COST-G solution after applying DDK5 (orange) and the CSR mascons solution (green).

#### *4.2.2 Method validation through regional hydrological mass balance*

To assess performances of our final GRACE/GRACE-FO M-SSA solution, compared to others, we seek validation through comparison with independent information at the regional scale, with the example of hydrological mass balance over reservoir impoundments. However, validating GRACE/GRACE-FO SH solutions comes with two major challenges.

Firstly, finding independent measurements of mass variations comparable to GRACE/GRACE-FO is difficult. Indeed, GRACE/GRACE-FO measures large scale combined variations in surface and groundwater, as well as within the solid Earth. In some regions, with minimal solid Earth related gravity variations, dense networks of groundwater measurements and available estimates of surface water components (snow, canopy, soil moisture) from other sources, namely models of land surface hydrology (ex: GLDAS, Rodell et al. (2004)), it has been possible to validate GRACE/GRACE-FO measurements (Scanlon et al., 2012; Feng et al., 2013). In addition, comparison with satellite altimetry, offers interesting opportunities to validate GRACE/GRACE-FO solutions. In particular, due its large spatial extent, significant signal amplitude and minimal groundwater variations in the region, the Caspian sea has become an ideal candidate to seek validation of mass change measurements with sea level variations measured by satellite altimetry (Swenson & Wahr, 2007; J. Chen et al., 2017). Unfortunately, the comparison of GRACE/GRACE-FO SH estimates at the regional scale with independent datasets suffers another challenge.

Any filtering strategy of the GRACE/GRACE-FO solutions, which is necessary to reduce North-South striping noise, causes spatial leakage error. This error is responsible for signal amplitude attenuation and causes geophysical signals to smear out over large regions. Reducing leakage bias is therefore essential to quantify mass variations at the regional scale, and requires independent sources of information. A commonly used method is the model-derived scaling factors, which model-dependency (Landerer & Swenson, 2012) can be overcome using data-driven methods (Vishwakarma et al., 2017; Dobslaw et al., 2020). Another well established method is forward modelling which uses *a priori* information on the source location to estimate the amplitude of the mass change through an iterative numerical scheme by minimising differences of the truncated and filtered GRACE/GRACE-FO data and *a priori* model until an arbitrary threshold criterion is met (J. Chen, Wilson, & Tapley, 2006; J. Chen, Wilson, Blankenship, & Tapley, 2006; J. Chen et al., 2015). The latter method has been used for various geophysical applications, from changes in ice mass (Wouters et al., 2008), lake water storage (J. Chen et al., 2017) or ocean mass (Jeon et al., 2018).

Here, we develop a modified forward modelling approach and apply it to reservoir impoundments, for which the shape and maximum volume capacity are well known. We first apply both filters used in our GRACE/GRACE-FO processing, namely DDK7 and LE, to the reservoir impoundment shape to obtain its theoretical filtered shape in the GRACE/GRACE-FO solution. We then perform, for each monthly gravity field, a linear regression between the DDK7+LE filtered GRACE/GRACE-FO observations and the filtered reservoir impoundment shape. The "true" reservoir impoundment volume variations are given by its actual surface times the time-dependent coefficient of the linear regression, and can be easily compared to its known capacity and date of commissioning.

In particular, we first consider the Boguchany Reservoir, impounded by a dam at Kodinsk, Russia, which is part of a major water storage system, including multiple dams on the Angara River, which flows out from Lake Baikal. The dam began to fill its reservoir in May 2012, with an expected maximum capacity of 58.2 $km^3$ of water (Jaguś et al., 2015). We also consider the Bakun embankment dam in Sarawak, Malaysia, on the Balui River (Oh et al., 2010, 2018), which started to be filled in late 2010, and reached its maximum capacity of 43.8 $km^3$ in 2011 (Tangdamrongsub et al., 2019). The Bakun

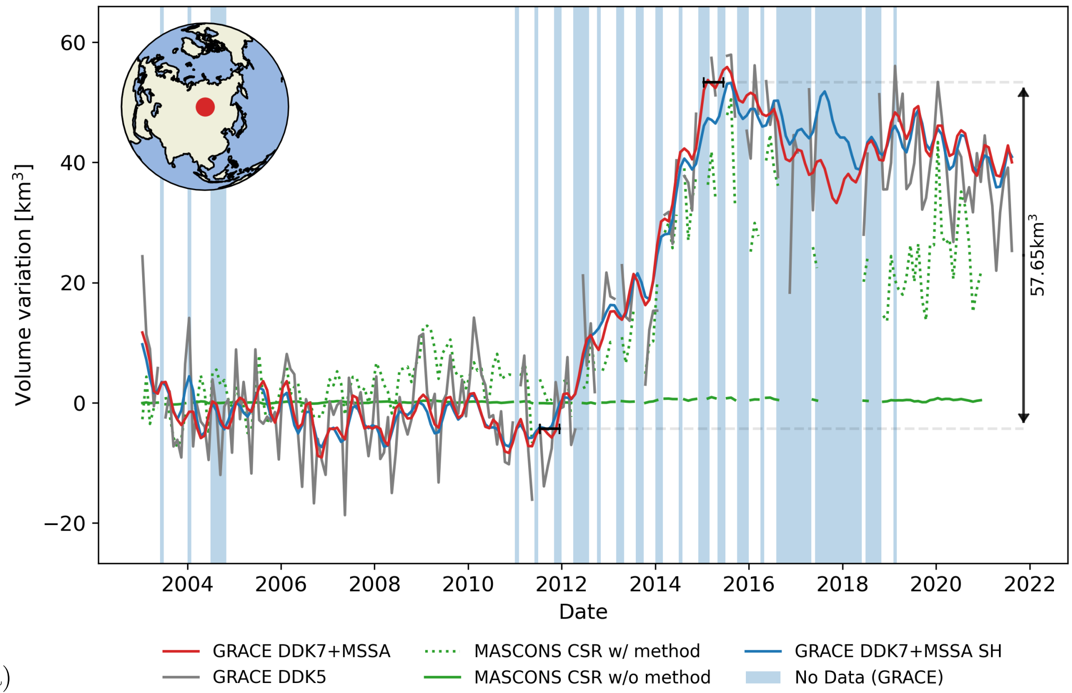


(a)

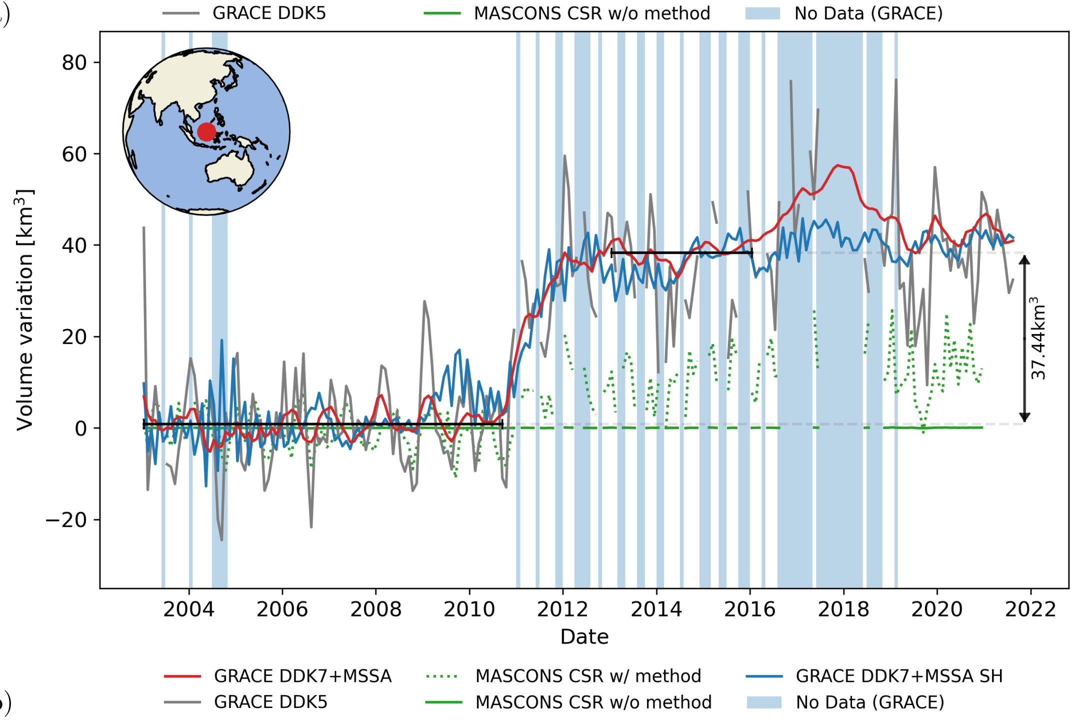


(b)

Figure 16: Volume variations of the (a) Boguchany Reservoir, impounded by a dam at Kodinsk, Russia, which reservoir began to be filled its reservoir in May 2012, with an expected maximum water capacity of 58.2 km$^3$ and (b) Bakun embankment dam in Sarawak, Malaysia, which started to be filled in late 2010, and maximum capacity of 43.8 km$^3$, associated with the close by Murum reservoir, which filling started in late 2014 for a maximum capacity of 12 km$^3$. Volume variations are computed using the modified forward model method proposed in this study, for the average of SH solutions processed by CSR, GRAZ, GFZ and JPL, filtered using DDK5 (gray), the M-SSA SH solution proposed by Prevost et al. (2019) and extended to GRACE-FO (blue), and our final GRACE/GRACE-FO M-SSA solution (red). Estimates are compared to volume variations derived from the CSR mascons solution at its expected spatial resolution (solid green), and using a larger area accounting for leakage error (dashed green), based on the forward model proposed for SH solutions.

dam has to be associated with the close by Murum reservoir, leading to non distinguishable signals at the GRACE/GRACE-FO spatial resolution. The Murum dam started to be filled in December 2014, up to its maximum capacity of 12.0 km $^3$. Figure 16 shows results of the method applied to several GRACE/GRACE-FO solutions for both reservoir impoundments. Particularly, we compared SH solutions using various filtering strategies, including the average of SH solutions processed by CSR, GRAZ, GFZ and JPL, filtered using DDK5, the M-SSA SH solution proposed by Prevost et al. (2019) and extended to GRACE-FO, and our final GRACE/GRACE-FO M-SSA solution. We also compare hydrological mass balance to CSR mascons solution, at its expected spatial resolution, and extending the mass balance over the same area used for SH solutions, i.e. accounting for leakage. SH solutions detect large mass variations related to reservoir impoundments for both Boguchany and Bakun reservoirs and the maximum volumes retrieved for the GRACE/GRACE-FO solution, over observing periods only, are 57.65 and 37.44 km$^3$. These results agree best with the true maximum capacity of the reservoirs, down to the 5 km$^3$ level. Note that we estimate the Bakun maximum capacity from GRACE/GRACE-FO solutions prior to the Murum lake filling to isolate its contribution. Moreover, since it is possible to characterize exactly the effect of both the DDK and LE filters on attenuation and leakage of a known source, regional mass balance based on SH solutions are consistent with independent datasets once corrected for these effects. Volumes retrieved using our final GRACE/GRACE-FO M-SSA solution are also larger than more filtered solutions, which emphasizes the ability of the method to recover smaller spatial wavelength signals with geophysical meaning. In contrast, volume retrieved by the CSR mascons solution at their expected spatial resolution are close to zero. When hydrological mass balance are performed over a larger area for CSR mascons, similar to the area used for SH solutions, we observe signals consistent with reservoir impoundments, but with a much lower amplitude than expected. This may be related to a significant regularisation of the CSR mascons solution in a region with little mass variations, and unexpected anthropogenic activity, and unknown exact transfer function between a known source and its mascons description which could impact regional mass budgets.

## 5 Conclusions

In this article we develop a post-processing strategy for gap filling, combining and filtering multiple GRACE/GRACE-FO Level-2 SH gravity field solutions, inspired by Prevost et al. (2019), with minimal *a priori* constraints on the signal or noise spatio-temporal evolution. First, we combine the DDK7 filter with a new Lobe-Edge filter, built to further reduce the remaining lobes of spurious errors, detected around spherical harmonic 40. We then perform gap filling of missing observations in times series of Equivalent Water Height (EWH) processed by 4 processing centres (CSR, GRAZ, GFZ, JPL), after identifying and removing outliers, and taking advantage of their common modes of variability using an iterative Multichannel Singular Spectrum Analysis (M-SSA). We then proceed to spatial filtering by applying the M-SSA on each averaged EWH time series, obtained from the 4 different solutions, and its near neighbours in the eastern and western directions to remove local striping artefacts.

We compare our final GRACE/GRACE-FO M-SSA solution with other solutions and seek ground truth through comparisons with independent observations. First, we ensure that gap filled periods, solely based on the iterative M-SSA scheme, are in agreement with low-degree Earth's gravity field derived from Satellite Laser Ranging and GLDAS, a surface land hydrology model. Comparisons show the M-SSA method ability to statistically reconstruct missing observations. Then, we investigate the noise content of the GRACE/GRACE-FO M-SSA solution over the oceans, which shows improvements compared to other spherical harmonic (SH) solutions, and a level similar to masons type solutions, that are regularized and/or constrained by construction. Finally, we show the potential of the method to retrieve short-wavelengths geophysical signals, often smeared out over large regions by highly filtered SH solutions or masked out by mascons solutions, using the example of hydrological mass balance of the Boguchany (Russia) and Bakun (Malaysia) reservoir impoundments. In turn, the GRACE/GRACE-FO M-SSA solution can reveal smaller spatial scale signals, including gravity changes induced by smaller melting glaciers or smaller magnitudes earthquakes.

## Acknowledgments

Level-2 GRACE and GRACE-FO data used in this study are freely available and provided by the Center of Space Reasearch (CSR) (https://podaac-tools.jpl.nasa.gov/drive/files/allData/grace/L2/CSR/RL06 and https://podaac-tools.jpl.nasa.gov/drive/files/allData/gracefo/L2/CSR/RL06), the GeoForschungsZentrum (GFZ) (https://podaac-tools.jpl.nasa.gov/drive/files/allData/grace/L2/GFZ/RL06 and https://podaac-tools.jpl.nasa.gov/drive/files/allData/gracefo/L2/GFZ/RL06.1, the Institute of Geodesy of the University of Graz (GRAZ) (http://ftp.tugraz.at/outgoing/ITSG/GRACE/ITSG-Grace2018/monthly/monthly_n96/ and http://ftp.tugraz.at/outgoing/ITSG/GRACE/ITSG-Grace_operational/monthly/monthly_n96/) and the Jet Propulsion Lavboratory (JPL) (https://podaac-tools.jpl.nasa.gov/drive/files/allData/grace/L2/JPL/RL06 and https://podaac-tools.jpl.nasa.gov/drive/files/allData/gracefo/L2/JPL/RL06). Stokes coefficient $C_{1,0}$ coefficients for GRACE and GRACE-FO are provided in the Technical Notes 13 ( https://podaac-tools.jpl.nasa.gov/drive/files/allData/grace/docs/). Stokes coefficients $C_{3,0}$ and $C_{5,0}$ are available in Technical Note 14 (https://podaac-tools.jpl.nasa.gov/drive/files/allData/gracefo/docs/TN-14_C30_C20_GSFC_SLR.txt). SLR data used for comparison are provided by CSR http://download.csr.utexas.edu/pub/slr/degree_5/CSR_Monthly_5x5_Gravity_Harmonics.txt and GLDAS is freely available at https://hydro1.gesdisc.eosdis.nasa.gov/data/GLDAS/GLDAS_NOAH10_M.2.1/GLDAS. Processing of the data has been done using `Python` (https://www.python.org/) using the M-SSA `pymssa` package (https://github.com/kieferk/pymssa) and `Python` interface for the Generic Mapping Tools `PyGMT` (https://www.pygmt.org/latest/). This study was supported by the CNES-TOSA HYDROGEODESY project. The final GRACE/GRACE-FO solution can be downloaded here `[link to be added upon publication]`.

## References


Allen, M., & Robertson, A. (1996). Distinguishing modulated oscillations from coloured noise in multivariate datasets. *Climate dynamics*, *12*(11), 775–784.

Argus, D. F., Peltier, W. R., Drummond, R., & Moore, A. W. (2014). The antarctica component of postglacial rebound model ice-6g_c (vm5a) based on gps positioning, exposure age dating of ice thicknesses, and relative sea level histories. *Geophysical Journal International*, *198*(1), 537–563.

Bonin, J. A., Bettadpur, S., & Tapley, B. D. (2012). High-frequency signal and noise estimates of csr grace rl04. *Journal of Geodesy*, *86*(12), 1165–1177.

Bouih, M., Panet, I., Remy, D., Longuevergne, L., & Bonvalot, S. (2022). Deep mass redistribution prior to the 2010 mw 8.8 maule (chile) earthquake revealed by grace satellite gravity. *Earth and Planetary Science Letters*, *584*, 117465.

Broomhead, D. S., & King, G. P. (1986). Extracting qualitative dynamics from experimental data. *Physica D: Nonlinear Phenomena*, *20*(2-3), 217–236.

Broomhead, D. S., King, G. P., et al. (1986). On the qualitative analysis of experimental dynamical systems. *Nonlinear phenomena and chaos*, *113*, 114.

Chambers, D. P. (2006). Observing seasonal steric sea level variations with grace and satellite altimetry. *Journal of Geophysical Research: Oceans*, *111*(C3).

Chambers, D. P., & Willis, J. K. (2008). Analysis of large-scale ocean bottom pressure variability in the north pacific. *Journal of Geophysical Research: Oceans*, *113*(C11).

Chanard, K., Fleitout, L., Calais, E., Rebischung, P., & Avouac, J.-P. (2018). Toward a global horizontal and vertical elastic load deformation model derived from grace and gnss station position time series. *Journal of Geophysical Research: Solid Earth*, *123*(4), 3225–3237.

Chen, J., Famigliett, J. S., Scanlon, B. R., & Rodell, M. (2016). Groundwater storage changes: present status from grace observations. In *Remote sensing and water resources* (pp. 207–227). Springer.

Chen, J., Rodell, M., Wilson, C., & Famiglietti, J. (2005). Low degree spherical harmonic influences on gravity recovery and climate experiment (grace) water storage estimates. *Geophysical Research Letters*, *32*(14).

Chen, J., Wilson, C., Blankenship, D., & Tapley, B. (2006). Antarctic mass rates from grace. *Geophysical research letters*, *33*(11).

Chen, J., Wilson, C., Famiglietti, J., & Rodell, M. (2007). Attenuation effect on seasonal basin-scale water storage changes from grace time-variable gravity. *Journal of Geodesy*, *81*(4), 237–245.

Chen, J., Wilson, C., Li, J., & Zhang, Z. (2015). Reducing leakage error in grace-observed long-term ice mass change: a case study in west antarctica. *Journal of Geodesy*, *89*(9), 925–940.

Chen, J., Wilson, C., & Tapley, B. (2006). Satellite gravity measurements confirm accelerated melting of greenland ice sheet. *science*, *313*(5795), 1958–1960.

Chen, J., Wilson, C., Tapley, B., Save, H., & Cretaux, J.-F. (2017). Long-term and seasonal caspian sea level change from satellite gravity and altimeter measurements. *Journal of Geophysical Research: Solid Earth*, *122*(3), 2274–2290.

Chen, J. L., Wilson, C. R., Tapley, B. D., & Grand, S. (2007). Grace detects coseismic and postseismic deformation from the sumatra-andaman earthquake. *Geophysical Research Letters*, *34*(13).

Cheng, M., Ries, J. C., & Tapley, B. D. (2011). Variations of the earth's figure axis from satellite laser ranging and grace. *Journal of Geophysical Research: Solid Earth*, *116*(B1).

De Viron, O., Diament, M., & Panet, I. (2006). Extracting low frequency climate signal from grace data. *eEarth Discussions*, *1*(1), 21–36.

Dobslaw, H., Bergmann-Wolf, I., Dill, R., Poropat, L., Thomas, M., Dahle, C., . . .

Flechtner, F. (2017). A new high-resolution model of non-tidal atmosphere and ocean mass variability for de-aliasing of satellite gravity observations: Aod1b rl06. *Geophysical Journal International*, *211*(1), 263–269.

Dobslaw, H., Dill, R., Bagge, M., Klemann, V., Boergens, E., Thomas, M., ... Flechtner, F. (2020). Gravitationally consistent mean barystatic sea level rise from leakage-corrected monthly grace data. *Journal of Geophysical Research: Solid Earth*, *125*(11), e2020JB020923.

Dong, D., Fang, P., Bock, Y., Cheng, M., & Miyazaki, S. (2002). Anatomy of apparent seasonal variations from gps-derived site position time series. *Journal of Geophysical Research: Solid Earth*, *107*(B4), ETG–9.

Feng, W., Zhong, M., Lemoine, J.-M., Biancale, R., Hsu, H.-T., & Xia, J. (2013). Evaluation of groundwater depletion in north china using the gravity recovery and climate experiment (grace) data and ground-based measurements. *Water Resources Research*, *49*(4), 2110–2118.

Flechtner, F., Neumayer, K.-H., Dahle, C., Dobslaw, H., Fagiolini, E., Raimondo, J.-C., & Güntner, A. (2016). What can be expected from the grace-fo laser ranging interferometer for earth science applications ? *Surveys in Geophysics*, *37*(2), 453–470.

Forootan, E., & Kusche, J. (2012). Separation of global time-variable gravity signals into maximally independent components. *Journal of Geodesy*, *86*(7), 477–497.

Forootan, E., Rietbroek, R., Kusche, J., Sharifi, M. A., Awange, J. L., Schmidt, M., ... Famiglietti, J. (2014). Separation of large scale water storage patterns over iran using grace, altimetry and hydrological data. *Remote Sensing of Environment*, *140*, 580–595.

Frappart, F., Ramillien, G., Leblanc, M., Tweed, S., Bonnet, M.-P., & Maisongrande, P. (2010). Continental water mass variations from independent component analysis (ica) of level-2 monthly grace data. In *Egu general assembly conference abstracts* (p. 5873).

Gardner, A. S., Moholdt, G., Cogley, J. G., Wouters, B., Arendt, A. A., Wahr, J., ... others (2013). A reconciled estimate of glacier contributions to sea level rise: 2003 to 2009. *science*, *340*(6134), 852–857.

Ghil, M., Allen, M., Dettinger, M., Ide, K., Kondrashov, D., Mann, M., ... others (2002). Advanced spectral methods for climatic time series. *Reviews of geophysics*, *40*(1), 3–1.

Guo, J., Duan, X., & Shum, C. (2010). Non-isotropic gaussian smoothing and leakage reduction for determining mass changes over land and ocean using grace data. *Geophysical Journal International*, *181*(1), 290–302.

Han, S.-C., Jekeli, C., & Shum, C. (2004). Time-variable aliasing effects of ocean tides, atmosphere, and continental water mass on monthly mean grace gravity field. *Journal of Geophysical Research: Solid Earth*, *109*(B4).

Humphrey, V., & Gudmundsson, L. (2019). Grace-rec: a reconstruction of climate-driven water storage changes over the last century. *Earth System Science Data*, *11*(3), 1153–1170.

Jäggi, A., Dahle, C., Arnold, D., Bock, H., Meyer, U., Beutler, G., & van Den Ijssel, J. (2016). Swarm kinematic orbits and gravity fields from 18 months of gps data. *Advances in Space Research*, *57*(1), 218–233.

Jäggi, A., Meyer, U., Lasser, M., Jenny, B., Lopez, T., Flechtner, F., ... others (2020). International combination service for time-variable gravity fields (cost-g) start of operational phase and future perspectives. Springer.

Jaguś, A., Rzętała, M. A., & Rzętała, M. (2015). Water storage possibilities in lake baikal and in reservoirs impounded by the dams of the angara river cascade. *Environmental Earth Sciences*, *73*(2), 621–628.

Jeon, T., Seo, K.-W., Youm, K., Chen, J., & Wilson, C. R. (2018). Global sea level change signatures observed by grace satellite gravimetry. *Scientific Reports*, *8*(1),

1–10.
Johnson, G. C., & Chambers, D. P. (2013). Ocean bottom pressure seasonal cycles and decadal trends from grace release-05: Ocean circulation implications. *Journal of Geophysical Research: Oceans*, *118*(9), 4228–4240.
Keppenne, C. L., & Ghil, M. (1993). Adaptive filtering and prediction of noisy multivariate signals: An application to subannual variability in atmospheric angular momentum. *International Journal of Bifurcation and Chaos*, *3*(03), 625–634.
Kondrashov, D., & Ghil, M. (2006a). Spatio-temporal filling of missing points in geophysical data sets. *Nonlinear Processes in Geophysics*, *13*(2), 151–159.
Kondrashov, D., & Ghil, M. (2006b, May). Spatio-temporal filling of missing points in geophysical data sets. *Nonlinear Processes in Geophysics*, *13*(2), 151-159.
Kondrashov, D., Shprits, Y., & Ghil, M. (2010). Gap filling of solar wind data by singular spectrum analysis. *Geophysical research letters*, *37*(15).
Kusche, J. (2007). Approximate decorrelation and non-isotropic smoothing of time-variable grace-type gravity field models. *Journal of Geodesy*, *81*(11), 733–749.
Kusche, J., Schmidt, R., Petrovic, S., & Rietbroek, R. (2009). Decorrelated grace time-variable gravity solutions by gfz, and their validation using a hydrological model. *Journal of geodesy*, *83*(10), 903–913.
Lai, Y., Zhang, B., Yao, Y., Liu, L., Yan, X., He, Y., & Ou, S. (2022). Reconstructing the data gap between grace and grace follow-on at the basin scale using artificial neural network. *Science of The Total Environment*, *823*, 153770.
Landerer, F. W., Flechtner, F. M., Save, H., Webb, F. H., Bandikova, T., Bertiger, W. I., … others (2020). Extending the global mass change data record: Grace follow-on instrument and science data performance. *Geophysical Research Letters*, *47*(12), e2020GL088306.
Landerer, F. W., & Swenson, S. (2012). Accuracy of scaled grace terrestrial water storage estimates. *Water resources research*, *48*(4).
Larochelle, S., Chanard, K., Fleitout, L., Fortin, J., Gualandi, A., Longuevergne, L., … Avouac, J.-P. (2022). Understanding the geodetic signature of large aquifer systems: Example of the ozark plateaus in central united states. *Journal of Geophysical Research: Solid Earth*, *127*(3).
Li, W., Wang, W., Zhang, C., Wen, H., Zhong, Y., Zhu, Y., & Li, Z. (2019). Bridging terrestrial water storage anomaly during grace/grace-fo gap using ssa method: A case study in china. *Sensors*, *19*(19), 4144.
Long, D., Longuevergne, L., & Scanlon, B. R. (2015). Global analysis of approaches for deriving total water storage changes from grace satellites. *Water Resources Research*, *51*(4), 2574–2594.
Longuevergne, L., Wilson, C., Scanlon, B., & Crétaux, J. (2013). Grace water storage estimates for the middle east and other regions with significant reservoir and lake storage. *Hydrology and Earth System Sciences*, *17*(12), 4817–4830.
Loomis, B., Luthcke, S., & Sabaka, T. (2019). Regularization and error characterization of grace mascons. *Journal of geodesy*, *93*(9), 1381–1398.
Loomis, B., Rachlin, K. E., Wiese, D. N., Landerer, F. W., & Luthcke, S. B. (2020). Replacing grace/grace-fo with satellite laser ranging: Impacts on antarctic ice sheet mass change. *Geophysical Research Letters*, *47*(3), e2019GL085488.
Lorenz, E. N. (1956). *Empirical orthogonal functions and statistical weather prediction* (Vol. 1). Massachusetts Institute of Technology, Department of Meteorology Cambridge.
Lück, C., Kusche, J., Rietbroek, R., & Löcher, A. (2018). Time-variable gravity fields and ocean mass change from 37 months of kinematic swarm orbits. *Solid Earth*, *9*(2), 323–339.
Luthcke, S. B., Sabaka, T., Loomis, B., Arendt, A., McCarthy, J., & Camp, J. (2013). Antarctica, greenland and gulf of alaska land-ice evolution from an iterated grace global mascon solution. *Journal of Glaciology*, *59*(216), 613–631.

Mémin, A., Boy, J.-P., & Santamaría-Gómez, A. (2020). Correcting gps measurements for non-tidal loading. *GPS Solutions*, *24*(2), 1–13.

Meyer, U., Jäggi, A., Jean, Y., & Beutler, G. (2016). Aiub-rl02: An improved time-series of monthly gravity fields from grace data. *Geophysical Journal International*, *205*(2), 1196–1207.

Meyer, U., Jean, Y., Kvas, A., Dahle, C., Lemoine, J.-M., & Jäggi, A. (2019). Combination of grace monthly gravity fields on the normal equation level. *Journal of geodesy*, *93*(9), 1645–1658.

Mo, S., Zhong, Y., Forootan, E., Mehrnegar, N., Yin, X., Wu, J., ... Shi, X. (2022). Bayesian convolutional neural networks for predicting the terrestrial water storage anomalies during grace and grace-fo gap. *Journal of Hydrology*, *604*, 127244.

Morison, J., Wahr, J., Kwok, R., & Peralta-Ferriz, C. (2007). Recent trends in arctic ocean mass distribution revealed by grace. *Geophysical Research Letters*, *34*(7).

Oh, T. H., Hasanuzzaman, M., Selvaraj, J., Teo, S. C., & Chua, S. C. (2018). Energy policy and alternative energy in malaysia: Issues and challenges for sustainable growth–an update. *Renewable and Sustainable Energy Reviews*, *81*, 3021–3031.

Oh, T. H., Pang, S. Y., & Chua, S. C. (2010). Energy policy and alternative energy in malaysia: Issues and challenges for sustainable growth. *Renewable and Sustainable Energy Reviews*, *14*(4), 1241–1252.

Panet, I., Mikhailov, V., Diament, M., Pollitz, F., King, G., De Viron, O., ... Lemoine, J.-M. (2007). Coseismic and post-seismic signatures of the sumatra 2004 december and 2005 march earthquakes in grace satellite gravity. *Geophysical Journal International*, *171*(1), 177–190.

Peltier, W. R., Argus, D., & Drummond, R. (2015). Space geodesy constrains ice age terminal deglaciation: The global ice-6g_c (vm5a) model. *Journal of Geophysical Research: Solid Earth*, *120*(1), 450–487.

Peltier, W. R., Argus, D. F., & Drummond, R. (2018). Comment on "an assessment of the ice-6g_c (vm5a) glacial isostatic adjustment model" by purcell et al. *Journal of Geophysical Research: Solid Earth*, *123*(2), 2019–2028.

Plaut, G., & Vautard, R. (1994). Spells of low-frequency oscillations and weather regimes in the northern hemisphere. *Journal of the atmospheric sciences*, *51*(2), 210–236.

Prevost, P., Chanard, K., Fleitout, L., Calais, E., Walwer, D., van Dam, T., & Ghil, M. (2019). Data-adaptive spatio-temporal filtering of grace data. *Geophysical Journal International*, *219*(3), 2034–2055.

Rangelova, E., Sideris, M., & Kim, J. (2012). On the capabilities of the multi-channel singular spectrum method for extracting the main periodic and non-periodic variability from weekly grace data. *Journal of geodynamics*, *54*, 64–78.

Rangelova, E., & Sideris, M. G. (2008). Contributions of terrestrial and grace data to the study of the secular geoid changes in north america. *Journal of Geodynamics*, *46*(3-5), 131–143.

Rangelova, E., Van der Wal, W., Braun, A., Sideris, M., & Wu, P. (2007). Analysis of gravity recovery and climate experiment time-variable mass redistribution signals over north america by means of principal component analysis. *Journal of Geophysical Research: Earth Surface*, *112*(F3).

Richter, H. M. P., Lück, C., Klos, A., Sideris, M. G., Rangelova, E., & Kusche, J. (2021). Reconstructing grace-type time-variable gravity from the swarm satellites. *Scientific reports*, *11*(1), 1–14.

Rieser, D., Kuhn, M., Pail, R., Anjasmara, I., & Awange, J. (2010). Relation between grace-derived surface mass variations and precipitation over australia. *Australian Journal of Earth Sciences*, *57*(7), 887–900.

Rietbroek, R., Fritsche, M., Dahle, C., Brunnabend, S.-E., Behnisch, M., Kusche, J., ... Dietrich, R. (2014). Can gps-derived surface loading bridge a grace mission

gap? *Surveys in Geophysics*, *35*(6), 1267–1283.
Rodell, M., Chen, J., Kato, H., Famiglietti, J. S., Nigro, J., & Wilson, C. R. (2007). Estimating groundwater storage changes in the mississippi river basin (usa) using grace. *Hydrogeology Journal*, *15*(1), 159–166.
Rodell, M., Houser, P., Jambor, U., Gottschalck, J., Mitchell, K., Meng, C.-J., ... others (2004). The global land data assimilation system. *Bulletin of the American Meteorological society*, *85*(3), 381–394.
Sakumura, C., Bettadpur, S., & Bruinsma, S. (2014). Ensemble prediction and intercomparison analysis of GRACE time-variable gravity field models. *Geophysical Research Letters*, *41*(5), 1389–1397.
Save, H., Bettadpur, S., & Tapley, B. D. (2012). Reducing errors in the grace gravity solutions using regularization. *Journal of Geodesy*, *86*(9), 695–711.
Save, H., Bettadpur, S., & Tapley, B. D. (2016). High-resolution csr grace rl05 mascons. *Journal of Geophysical Research: Solid Earth*, *121*(10), 7547–7569.
Scanlon, B. R., Longuevergne, L., & Long, D. (2012). Ground referencing grace satellite estimates of groundwater storage changes in the california central valley, usa. *Water Resources Research*, *48*(4).
Schrama, E. J., Wouters, B., & Lavallée, D. A. (2007). Signal and noise in gravity recovery and climate experiment (grace) observed surface mass variations. *Journal of Geophysical Research: Solid Earth*, *112*(B8).
Seo, K.-W., Wilson, C., Famiglietti, J., Chen, J., & Rodell, M. (2006). Terrestrial water mass load changes from gravity recovery and climate experiment (grace). *Water Resources Research*, *42*(5).
Seo, K.-W., Wilson, C. R., Chen, J., & Waliser, D. E. (2007). Grace's spatial aliasing error. *Geophysical Journal International*, *172*(1), 41–48.
Sośnica, K., Jäggi, A., Meyer, U., Thaller, D., Beutler, G., Arnold, D., & Dach, R. (2015). Time variable earth's gravity field from slr satellites. *Journal of geodesy*, *89*(10), 945–960.
Steffen, H., Denker, H., & Müller, J. (2008). Glacial isostatic adjustment in fennoscandia from grace data and comparison with geodynamical models. *Journal of Geodynamics*, *46*(3-5), 155–164.
Sun, Y., Riva, R., & Ditmar, P. (2016). Optimizing estimates of annual variations and trends in geocenter motion and j2 from a combination of grace data and geophysical models. *Journal of Geophysical Research: Solid Earth*, *121*(11), 8352–8370.
Swenson, S., Chambers, D., & Wahr, J. (2008). Estimating geocenter variations from a combination of grace and ocean model output. *Journal of Geophysical Research: Solid Earth*, *113*(B8).
Swenson, S., & Wahr, J. (2002). Methods for inferring regional surface-mass anomalies from gravity recovery and climate experiment (grace) measurements of time-variable gravity. *Journal of Geophysical Research: Solid Earth*, *107*(B9), ETG–3.
Swenson, S., & Wahr, J. (2006). Post-processing removal of correlated errors in grace data. *Geophysical Research Letters*, *33*(8).
Swenson, S., & Wahr, J. (2007). Multi-sensor analysis of water storage variations of the caspian sea. *Geophysical Research Letters*, *34*(16).
Syed, T. H., Famiglietti, J. S., Rodell, M., Chen, J., & Wilson, C. R. (2008). Analysis of terrestrial water storage changes from grace and gldas. *Water Resources Research*, *44*(2).
Tangdamrongsub, N., Han, S.-C., Jasinski, M. F., & Šprlák, M. (2019). Quantifying water storage change and land subsidence induced by reservoir impoundment using grace, landsat, and gps data. *Remote Sensing of Environment*, *233*, 111385.
Tapley, B. D., Bettadpur, S., Ries, J. P., Thompson, P. F., & Watkins, M. M. (2004). Grace measurements of mass variability in the earth system. *Science*, *305*(5683), 503–505.

Thompson, P., Bettadpur, S., & Tapley, B. (2004). Impact of short period, non-tidal, temporal mass variability on grace gravity estimates. *Geophysical research letters*, *31*(6).

Velicogna, I., Mohajerani, Y., Landerer, F., Mouginot, J., Noel, B., Rignot, E., … Wiese, D. (2020). Continuity of ice sheet mass loss in greenland and antarctica from the grace and grace follow-on missions. *Geophysical Research Letters*, *47*(8), e2020GL087291.

Velicogna, I., & Wahr, J. (2013). Time-variable gravity observations of ice sheet mass balance: Precision and limitations of the grace satellite data. *Geophysical Research Letters*, *40*(12), 3055–3063.

Vianna, M. L., Menezes, V. V., & Chambers, D. P. (2007). A high resolution satellite-only grace-based mean dynamic topography of the south atlantic ocean. *Geophysical Research Letters*, *34*(24).

Vishwakarma, B. D., Horwath, M., Devaraju, B., Groh, A., & Sneeuw, N. (2017). A data-driven approach for repairing the hydrological catchment signal damage due to filtering of grace products. *Water Resources Research*, *53*(11), 9824–9844.

Wahr, J., Swenson, S., Zlotnicki, V., & Velicogna, I. (2004). Time-variable gravity from grace: First results. *Geophysical Research Letters*, *31*(11).

Walwer, D., Calais, E., & Ghil, M. (2016). Data-adaptive detection of transient deformation in geodetic networks. *Journal of Geophysical Research: Solid Earth*, *121*(3), 2129–2152.

Wang, F., Shen, Y., Chen, Q., & Wang, W. (2021). Bridging the gap between grace and grace follow-on monthly gravity field solutions using improved multichannel singular spectrum analysis. *Journal of Hydrology*, *594*, 125972.

Wang, F., Shen, Y., Chen, T., Chen, Q., & Li, W. (2020). Improved multichannel singular spectrum analysis for post-processing grace monthly gravity field models. *Geophysical Journal International*, *223*(2), 825–839.

Wang, X., de Linage, C., Famiglietti, J., & Zender, C. S. (2011). Gravity recovery and climate experiment (grace) detection of water storage changes in the three gorges reservoir of china and comparison with in situ measurements. *Water Resources Research*, *47*(12).

Watkins, M. M., Wiese, D. N., Yuan, D.-N., Boening, C., & Landerer, F. W. (2015). Improved methods for observing earth's time variable mass distribution with grace using spherical cap mascons. *Journal of Geophysical Research: Solid Earth*, *120*(4), 2648–2671.

Werth, S., Güntner, A., Schmidt, R., & Kusche, J. (2009). Evaluation of grace filter tools from a hydrological perspective. *Geophysical Journal International*, *179*(3), 1499–1515.

Wouters, B., Chambers, D., & Schrama, E. (2008). Grace observes small-scale mass loss in greenland. *Geophysical Research Letters*, *35*(20).

Wouters, B., Gardner, A. S., & Moholdt, G. (2019). Global glacier mass loss during the grace satellite mission (2002-2016). *Frontiers in earth science*, *7*, 96.

Wouters, B., Riva, R., Lavallée, D., & Bamber, J. (2011). Seasonal variations in sea level induced by continental water mass: First results from grace. *Geophysical Research Letters*, *38*(3).

Wouters, B., & Schrama, E. J. (2007). Improved accuracy of grace gravity solutions through empirical orthogonal function filtering of spherical harmonics. *Geophysical Research Letters*, *34*(23).

Wu, X., Haines, B. J., Heflin, M. B., & Landerer, F. W. (2020). Improved global nonlinear surface mass variation estimates from geodetic displacements and reconciliation with grace data. *Journal of Geophysical Research: Solid Earth*, *125*(2), e2019JB018355.

Yang, X., Tian, S., You, W., & Jiang, Z. (2021). Reconstruction of continuous grace/grace-fo terrestrial water storage anomalies based on time series decomposition. *Journal of Hydrology*, *603*, 127018.

Yi, S., & Sneeuw, N. (2021). Filling the data gaps within grace missions using singular spectrum analysis. *Journal of Geophysical Research: Solid Earth*, *126*(5), e2020JB021227.

Zotov, L., & Shum, C. (2010). Multichannel singular spectrum analysis of the gravity field data from grace satellites. In *Aip conference proceedings* (Vol. 1206, pp. 473–479).